Repurposing of Artesunate and its derivative as antivirals against Japanese Encephalitis Virus infection

Dissertation report submitted to the National Brain Research Centre for the partial fulfilment of the requirements of Master of Science (M.Sc.) in Neuroscience

Submitted by

AASHI

Supervisor

Dr. Anirban Basu

Division of Cellular and Molecular Neuroscience,

National Brain Research Centre,

Manesar, Haryana, India

ब्रिक – राष्ट्रीय मस्तिष्क अनुसंधान केंद्र
BRIC – National Brain Research Centre
(जैव प्रौद्योगिकी अनुसंधान एव नवाचार परिषद, भारत सरकार)
एन० एच०–08, मानेसर–122 052 (हरियाणा), भारत
(An Institute of the Biotechnology Research and Innovation Council, Govt. of India)
NH-08, Manesar - 122 052 (Haryana), INDIA

CERTIFICATE

This is to certify that the thesis entitled **"Repurposing of Artesunate and its derivative as antivirals against Japanese Encephalitis Virus infection"** is the result of work carried out by **Aashi** in the Division of Cellular and Molecular Neuroscience, National Brain Research Centre, Manesar, Haryana, India for the partial fulfillment of requirements for the M.Sc. degree.

The work presented herein is original and has not been submitted previously for the award of any degree or diploma to **National Brain Research Centre (Deemed University)** or to any other university. This work is as per the guidelines given by **National Brain Research Centre (Deemed University)** and is a record of candidate's own efforts.

Dr. Anirban Basu
(Supervisor)

Dr. Sagar Sengupta
Director (Additional Charge)

Place: Manesar

Date: 16/06/2025

दूरभाष / Telephone : +91-124-2845200 फैक्स / Fax : +91-124-2338910
ई-मेल / E-mail : info.nbrc@nbrc.ac.in Website : www.nbrc.ac.in

DECLARATION

I **Aashi** hereby declare that the work presented in the dissertation entitled "Repurposing of Artesunate and its derivative as antivirals against Japanese Encephalitis Virus infection" is carried out solely by me under the guidance of Dr. Anirban Basu, at **National Brain Research Centre (Deemed to be University),** Manesar, Haryana, India.

I also declare that no part of this dissertation has been previously submitted for the award of any degree or diploma to National Brain Research Centre or any other University.

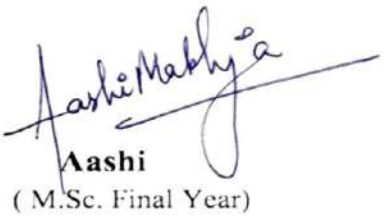

Place : Manesar
Date : 12-06-2025

Aashi
(M.Sc. Final Year)

Acknowledgment

"Every researcher's path is lit by mentors, peers, and moments of quiet clarity. This section is for the ones who lit mine."

First and foremost, I wish to express my deepest gratitude to my supervisor, **Dr. Anirban Basu**, (Scientist VII) in the Division of Cellular and Molecular Neuroscience, National Brain Research Centre for his invaluable guidance, support, and insightful mentorship throughout the course of this research. His scientific vision, patience, and encouragement have played a pivotal role in shaping this project. I also greatly appreciate his and Dr. Ellora Sen's encouragement towards mindful eating and healthy living, something which often added a refreshing dimension to our interactions. What I am especially grateful for is his ability to nurture interests beyond the bench which has played a vital role in broadening my outlook on career and life in whole.

I would like to extend my gratitude to **Dr. Ugir Hossain SK**, Chittaranjan National Cancer Institute, Kolkata, West Bengal for their invaluable collaboration in synthesizing Compound 9, which formed the very foundation of my dissertation study. I am also grateful to his team especially Rubi Roy and Debapriya Roymahapatra for their expertise and timely support at all required times.

I am sincerely grateful to my mentor Anirudh S. ~ you've been a true guide, motivate or, and a constant support. Your patience in answering my endless questions and your generosity in sharing your knowledge never went unnoticed. Despite our completely mismatched circadian rhythms, your coordinated effort and support helped me to finish daily tasks seamlessly. I greatly admire your patience while you corrected my mistakes, creating an encouraging learning space and better emotional well-being. Your presence has been an invaluable part of this thesis.

I feel truly blessed to have very encouraging and supportive parents Mrs. Ginny and Mr. Naresh Kumar and my little packets of joyful strength, my siblings (Mishthi and Ramsharan) for being my strongest pillars and true reflectors—your constant love, understanding, and motivation have been my foundation. I'm greatly thankful to each and every member of my family for always standing by me and for always being eager to resolve any and every minor inconvenience I faced.

A heartfelt thanks to my current labmates~ Komolika Di, Akasmika Di, Maygha, Rajyashree and recent lab alumni — Indira Di, Meenakshi Di and Atreye Di for their countless discussions, technical help, shared workload and frustrations that eventually ended up with louder laughs at cafetaria table and made long days at the lab bench feel lighter. Especially to Akasmika Di, your observations and inputs have been really instrumental in improving my benchwork skills. It has been a great research experience, I've learned so much simply by watching you work. Also this project won't have come up this early and beautifully without Shreya Basu, what an energetic boost of motivation you have been, truly one of the best companions I could ever ask for.

For a journey that would have been all the bumpier otherwise, I feel truly fortunate to have come across two angel souls—Anshu Gupta and Saurabh Bajpayee. Your constant presence, whether it was patiently listening to my rants at the most unusual hours or lifting my spirits during moments of exhaustion and doubt, made an immense difference. The flavourful food with condiments of reality checks, encouragement and humour that we share have helped me navigate life with far more ease and optimism than I could have ever managed on my own. Also I would like to thank Hamdaan and Anshika for their cheerful, energetic support in end work compilation.

I would also like to thank Kanhaiya bhaiya and Manish bhaiya, for their timely motivation, small talks and without whom I couldn't have carried out my everyday experiments with ease. Lastly, I owe my regards to all of my batchmates for a bunch of unique personalities everyone brought, each inspiring in its own way and to Vibha for all the odd time discussions and being a great roommate.

Each of you, in your own way, has contributed immensely to my scientific and personal growth. I remain deeply grateful.

ABBREVIATIONS

BBB	Blood Brain Barrier
BCA	Bicinchoninic Acid
BSA	Bovine Serum Albumin
cDNA	complementary Deoxyribonucleic Acid
CNS	Central Nervous System
CO_2	Carbon Dioxide
CSF	Cerebrospinal Fluid
JEV	Japanese Encephalitis Virus
DMEM	Dulbecco's Modified Eagle's Medium
DMSO	Dimethyl Sulphoxide
EB	Electrode Buffer
RPM	Rotation per Minute
RT	Room Temperature
SDS	Sodium Dodecyl Sulphate
SOV	Sodium Ortho-vanadate

WNV	West Nile Virus
TB	Transfer Buffer
TBST	Tris Buffer with triton X-100
TEMED	Tetra-methyl-ethylenediamine
β –ACTIN	Beta - Actin
β- ME	Beta Mercapto-ethanol
p-NFκB	phospho-Nuclear factor kappa chain B cell

ABSTRACT

Japanese Encephalitis Virus (JEV), a mosquito borne zoonotic virus remains a significant public health concern as it causes severe Encephalitis and due to limited therapeutic options available, JEV epidemics have resulted in significant morbidity and mortality rates. Artesunate (Art), a semi-synthetic derivative of artemisinin has shown modest antiviral potential; however, its efficacy against neurotropic viral infections like JEV is not optimal. In this study, we investigated a novel derivative of Art i.e. Compound 9 (C9), for its antiviral and neuroprotective potential primarily using *in vitro* and further *in vivo* models.

In vitro, C9 demonstrated superior efficacy over Art in reducing viral replication of NS3, preserving cell viability, and mitigating oxidative. C9 significantly reduced reactive oxygen species (ROS) and nitric oxide (NO) levels in infected neuronal cell lines and effectively decreased apoptosis as quantified by Annexin-V/PI staining. Immunocytochemistry further confirmed a greater reduction in the number of JEV-infected cells with C9, especially at lower concentrations, indicating a stronger and more dose-efficient antiviral effect.

In vivo, C9 and Art treatment markedly improved survival outcomes in JEV-infected BALB/c mice. Survival analysis using the log-rank Mantel-Cox test confirmed statistically significant protection, especially at 7 and 10 mg/kg doses not only enhanced the protection from JEV induced Encephalitis but also helped in the early and better revival of JEV symptoms. Additionally, C9-treated mice maintained better body weight profiles, suggesting improved overall health and reduced disease burden.

Together, these results underscore the enhanced antiviral, antioxidant, and anti-apoptotic properties of Compound 9, positioning it as a promising lead candidate for therapeutic intervention against JEV. Its improved efficacy over Artesunate across all experimental readouts supports further development and validation in ongoing preclinical models.

List of Figures

Fig 2.1.	Classification of arbovirus (Adapted from Srichawla et al,2024)
Fig 2.2.	Different mechanisms of viral entry in the CNS (Adapted from Srichawla et al, 2024)
Fig 2.3.	Viral replication complex at the ER (Adapted from Ci et al 2021)
Fig 2.4.	Reported JEV infection in humans mapped across the geography (Adapted from Oliveira et al 2020)
Fig 2.5.	Representation of JEV structural and genomic organization (Adapted from Sharma et al, 2021)
Fig 5.1.	Structural conformation of compound 9 by ^{1}H-NMR
Fig 5.2.	Cytotoxic profile of Artesunate and Compound 9
Fig 5.3.	Artesunate and Compound 9 treatment reduced viral RNA expression and JEV-NS3 protein expression
Fig 5.4.	Representative ICC images showing NS3 positive cells
Fig 5.5.	Artesunate and Compound 9 reduced JEV-induced oxidative stress and inflammation
Fig 5.6.	Annexin V/PI staining indicating attenuated JEV-induced apoptosis post treatment
Fig 5.7.	In-vivo efficacy of Art and C9 Treatment against JEV

CONTENTS

CHAPTER - 1	INTRODUCTION	12-13
CHAPTER - 2	LITERATURE SURVEY	14-32
CHAPTER - 3	AIM OF THE STUDY	33
CHAPTER – 4	MATERIAL AND METHODS	34-48
CHAPTER - 5	RESULTS	49-67
CHAPTER - 6	DISCUSSION	68-71
CHAPTER - 7	CONCLUSION	72
	APPENDICES	73-74
	LIST OF TABLES	75
	REFRENCES	76-83

Chapter 1

INTRODUCTION

Japanese Encephalitis Virus (JEV) is a positive-sense, single-stranded (ss) RNA virus that is the leading cause of acute viral encephalitis in Southeast Asia and the Western Pacific regions. It is a mosquito-borne flavivirus and belongs to the same genus as dengue, Zika, yellow fever, and West Nile viruses. JEV genome encodes for three structural and seven non-structural proteins critical for viral replication and pathogenesis. While the majority of cases occur in children below 15 years of age, JEV primarily targets the central nervous system, leading to high mortality rates and causing a heavy socio-economic burden. Despite the available vaccination programs, there is no cure for the disease, and the demand for antiviral treatments remains significant, especially for managing severe clinical signs of acute infections and related complications.

Artesunate, one of the semisynthetic derivatives of artemisinin type sesquiterpene lactones from Artemisia annua L., was originally identified as a potent antimalarial agent. While its bioactivity has been explored extensively for anti-cancer and virus inhibition potential. As literature supports the evidence for structural and functional attributes of C9, its ability to mitigate JEV-induced inflammation and viral replication offers an avenue for therapeutic exploration. Recently, artesunate has been repurposed to form an azide-substituted hybrid molecule i.e. Compound 9 (C9). The further set of experiments aims to elucidate the therapeutic potential of C9 in comparison to traditional artesunate using an *in vitro* HT22 neuronal cell line and further in an *in vivo* BALB/c mouse. C9/Art was administered 24 hours post-infection for comparative analysis between various drug doses and with their untreated counterparts. Utilizing the modified artesunate derivative C9, this study contributes to the development of innovative therapeutic strategies against JEV and expands the scope of artemisinin derivatives in combating viral diseases.

Chapter 2

LITERATURE SURVEY

2.1 Viruses and neurotropic infections

Viruses are obligate intracellular parasites composed of nucleic acid (DNA or RNA) encased in a protein capsid, and in some cases, a lipid envelope. Lacking cellular structures, they rely entirely on host cell machinery for replication[1]. The viral replication cycle involves adsorption, penetration, uncoating, biosynthesis, assembly, and release. They can significantly impact the central nervous system (CNS) through direct infection, immune-mediated damage, or disruption of neural homeostasis. RNA viruses, due to their high mutation rates, exhibit rapid evolution and antigenic variability, causing major epidemic outbreaks and a threat to the healthcare system worldwide[2].

Among the viral families that impact CNS pathology, five arbovirus families i.e. *Flaviviridae, Rhabdoviridae, Togaviridae, Bunyaviridae, and Reoviridae* are most studied. These groups of viruses use arthropods (mainly *Culex* mosquitoes) as vectors for viral transmission[3]. Using early classification of virus, based on tissue or organ tropism, viral infections by members of these families, especially *Flaviviridae,* fall under two broad categories- viscerotropic and neurotropic, some have features of both. While viscerotropic infections (caused by Dengue Virus, Yellow Fever Virus) primarily affect internal organs and systems like the liver, vascular endothelium. Neurotropic viruses (Japanese encephalitis virus, West Nile virus) preferentially infect the central nervous system[4]. Microscopic examination of the virus infected brains reveals neuronal cell death, activation of microglia, infiltration of macrophages, and the accumulation of CD4+ and CD8+ T cells.[2]

Within the family *Flaviviridae*, tick-borne encephalitis virus (TBEV), JEV and WNV causes severe encephalitis, meningitis, and paralysis like symptoms in infected patients across the Southern and Eastern parts of Asia.

In family *Togaviridae,* Alphaviruses cause encephalomyelitis in humans with neurological sequelae, signs of meningitis, and reduced consciousness. Genus Bunyavirus includes La Crosse, and California serogroup viruses, which upon infection cause severe encephalitis with meningeal signs, seizures, and epilepsy, whereas patients with Colorado Tick fever (Family *Reoviridae*) displays features of reduced consciousness and photophobia with rare development of encephalitis[5,6].

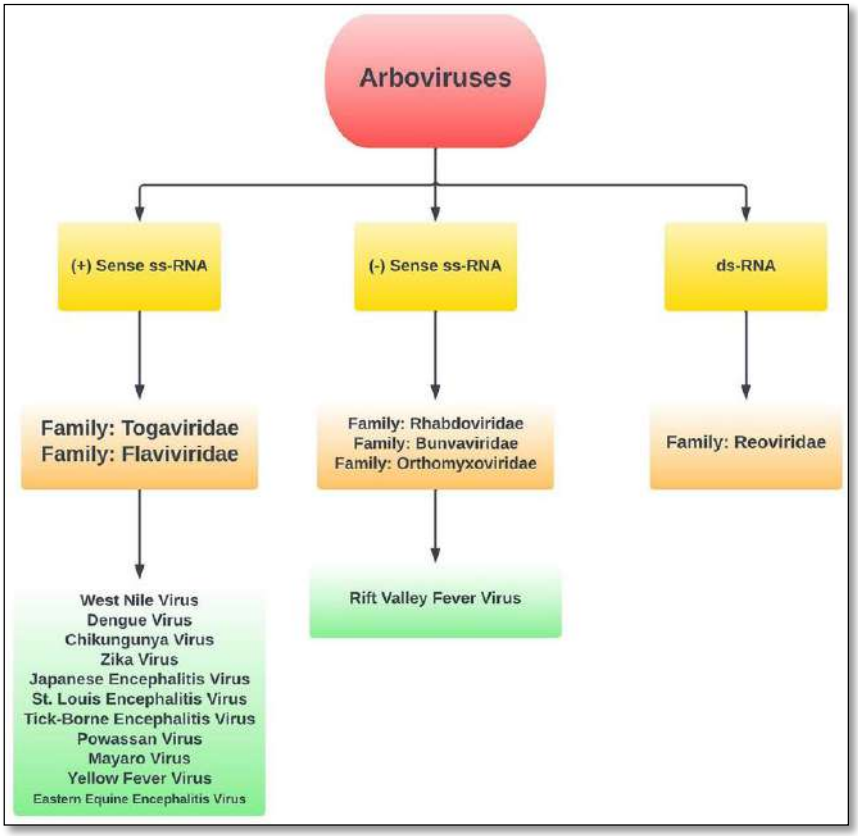

Fig 2.1. Classification of arbovirus (Adapted from Srichawla et al, 2024)

Most neurotropic infections are accidental or opportunistic, except a few which have adapted to infectthe nervous system efficiently (Alpha herpes virus and rabies). As the regeneration capacity of the brain and spinal cord tissue is limited, the tissue damage in the

CNS due to viral infections causes a plethora of neuropsychiatric sequelae. If further progressed, neurotropic viruses might become latent and appear later in life, causing multiple sclerosis, Guillain-Barré syndrome(GBS) , Shingles, and lethargic encephalitis[3].

2.2 CNS invasion and viral progression

While there are several routes by which neurotropic viruses such as the JEV gets access to the CNS[6] (Fig 2), it is still unclear if they coexist or dominate over each other. The most common mode of viral entry is the retrograde transport of the virus, wherein the virus enters the peripheral nerve endings and gets transported to the spinal cord and brain. Rabies virus and Herpes simplex virus (HSV) enter through this route[7,8]. Another route of viral entry into the CNS is via olfactory neurons, which upon being infected, transport viruses such as SARS-Cov-2 and influenza in anterograde fashion to axon bundles of the olfactory bulb, from where the virus spreads to other regions of the brain[9].

Alternatively, the "Trojan horse" mechanism, wherein virions hide themselves inside immune defense cells, is reported as a viral entry method. Viral species primarily infect the circulating lymphocytes of the blood that naturally enter and exit the CNS leading to a hematogenous viral spread-which get transported to neurons through endothelial cells and glia limitans[10].Disruption of the blood-brain barrier (BBB) due to local inflammation caused by viral infection also allows this free movement of virion particles or infected lymphocytes across the CNS. Alternatively, brain parenchyma and neurons have also been reported to get infected after initial viral replication in endothelial cells.

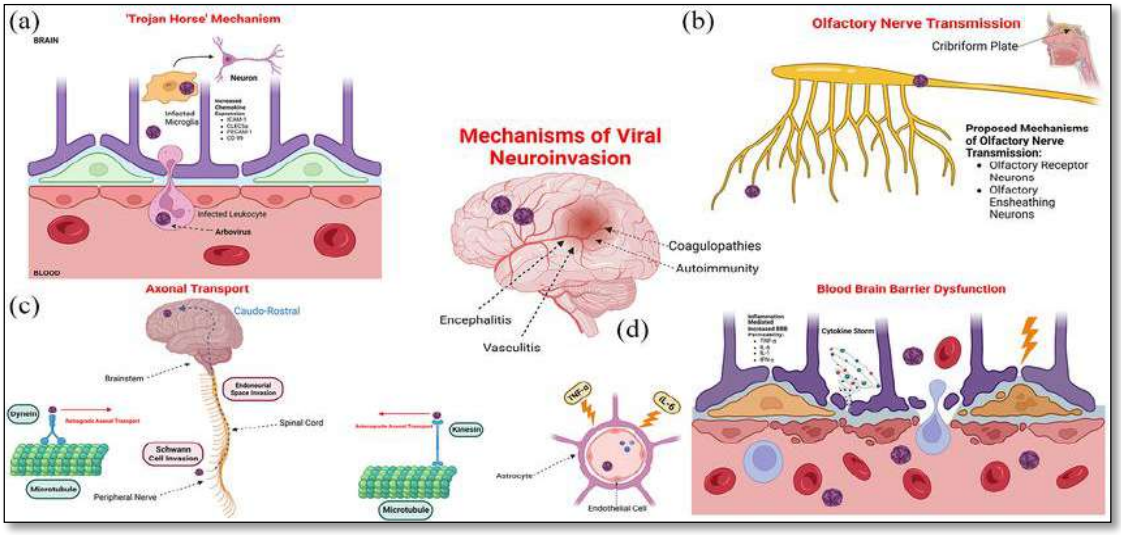

Fig 2.2. Different mechanisms of viral entry in the CNS indicating the "Trojan horse" mechanism, olfactory nerve transmission, axonal transport, and blood-brain barrier dysfunction. (Adapted from Srichawla et al, 2024)

2.2.1 Initiation of infection

Neurons, as compared to typical mammalian cells are highly polarized with long, distinct-axonal processes and extended dendrites. Communication across distal axons and their cell bodies require a highly specialized intracellular system or membrane-initiated signaling[10].

Neurotropic viruses enter host cells by endocytosis using specific cellular receptors that remain concentrated in the cellular membrane. Generally, two types of surface structures play an important role in the viral entry. First, the attachment factors that help to concentrate viruses near the cellular surface, such as glycosaminoglycan (GAG) and proteoglycans act as attachment factors for JEV[11]. Second, there are multiple viral receptors that actively promote viral entry by endocytosis (CD4, PLVAP, and GKN3 act as cellular receptors for JEV)[12].

The molecular mechanisms of endocytosis of flaviviruses (JEV and WNV) have already been studied in various cell types; however, similar studies using CHPV remain extremely limited.

In brief, neuronal endocytosis, when compared to non neuronal cells, is highly regulated by the conserved machinery of clathrin-coated vesicles[13,14].

Upon entry, the viral membrane destabilizes when exposed to the acidic milieu of the late endosome and releases the viral nucleocapsid in the cytoplasm. As the capsid protein protect and stabilizes the viral genome, viral RNA needs to be uncoated from the associated proteins for undergoing translation. This is performed using host ubiquitylation enzymes which translate the viral RNA genome into its polyprotein[15].

2.2.2 Genome Replication

Viruses rely on host ribosomal machinery for translating viral genome. Initially translated viral replication proteins act the template for synthesizing new genomic RNA strands for viral progeny[15,16]. The majority of RNA viruses that replicate within cytoplasm, remodel and compartmentalize host's Endoplasmic Reticulum using various non-structural (NS) viral proteins, thus forming the replication complexes (RC) to replicate the viral genome efficiently and protect themselves from the host's antiviral defense system. Cryo-EM has revealed the ultrastructure of these RCs, briefing invaginations of ER during JEV[17].

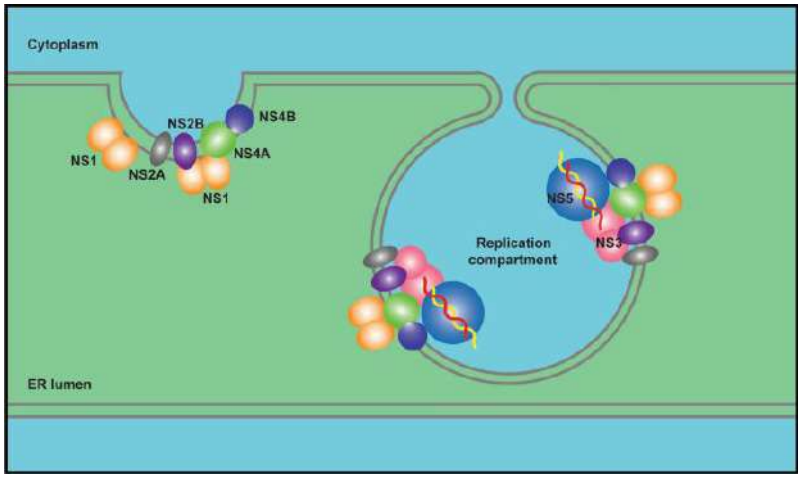

Fig 2.3. Viral replication complex at the ER (Adapted from Ci et al 2021)

2.2.3 Egress and spread

Most neurotropic viruses spread along the chains of inter-connected neurons in CNS via close cell-cell contact or synapses[10]. Assembly of an enveloped virus from the ER membrane requires two additional steps before egressing the mature viral particles through the Golgi :-

1. nucleocapsid formation (also called as encapsidation) and
2. Viral budding (envelope acquisition).

Apart from being transported from different sub-assemblies, viral assembly and egress are highly coordinated processes in which nucleocapsids and membrane proteins simultaneously converge at the plasma membrane[15].

2.3. Japanese Encephalitis Virus (JEV)

Japanese Encephalitis Virus (JEV) is a positive-sense, single-stranded enveloped mosquito-borne flavivirus that causes Japanese Encephalitis (JE), a leading cause of viral encephalitis in Asia. It is transmitted primarily by *Culex* mosquitoes, with pigs and water birds serving as amplifying hosts. While JEV is endemic in parts of Asia and the Western Pacific, unintentional transport of vectors from endemic areas to a new geographical location causes frequent outbreaks especially in rural areas with rice fields and pig farming, where mosquitoes thrive. Most infections are asymptomatic, but severe cases can lead to high fever, seizures, coma, and death (reportedly in 30% of cases), or if survived, it causes permanent neurological damage. While there is no specific antiviral treatment, vaccination remains the most effective preventive measure[18].

2.3.1 Epidemiology and transmission cycle

JEV widely occurs across the eastern and southern Asian countries as it circulates among wild wading birds. Transmission of JEV is maintained between various mosquitoes, water birds and vertebrates (Enzootic cycle), where egret and pond herons act as natural reservoir for JEV. Pigs act as an amplifying host and humans as dead end hosts[18,19].

Although JEV has been reported to be present in more than 30 species of mosquitoes which includes Aedes, Anopheles, Culex, and Mansonia. *Culex vishnui* and *Culex Tritaeniorhynchus* remains its primary vector as it is related to agricultural practices like rice cultivation or irrigated crop fields[20].JEV Infection in vertebrates like pigs and horses generally remains subclinical with no signs of disease complications as they develop persistently high viral load or viremia for up to 5 days. During this viremia phase, if a *Culex* mosquito feeds blood meal on one of these infected animals, it becomes infected with JEV followed by virus replication in the salivary glands of the infected mosquito. Mosquitoes can bite and introduce JEV in an immunologically naïve host vertebrate, thus completing the cycle of JEV infection[21].

Reports suggest that JEV also has the capacity for non-vector transmission between infected and naive pigs via the respiratory secretions without any physical contact[22]. Humans and large vertebrates like cattle living in close proximity with amplifying hosts get infected due to low viremia in the peripheral blood and serve as the accidental host/dead-end host for JEV[23]. Additionally, the geographical range of the *Culex* mosquito is expected to expand, due to the ongoing increased average temperature and varying precipitation patterns owing to global warming[24].

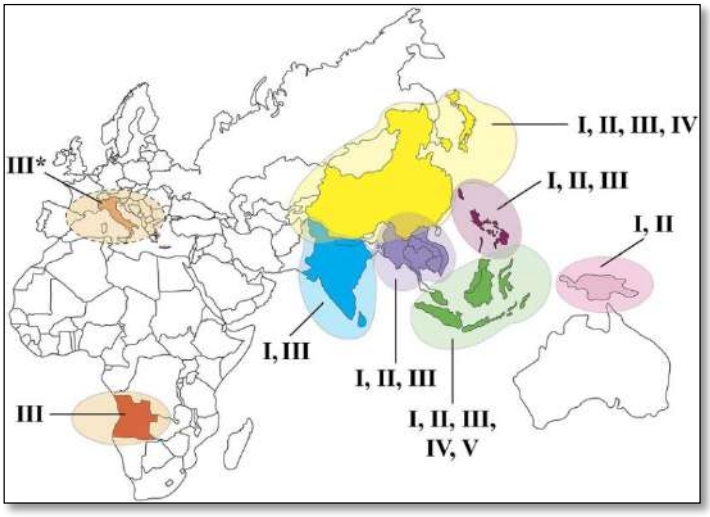

Fig 2.4. Reported JEV infection in humans mapped across the geography

(Adapted from Oliveira et al 2020)

Epidemiological patterns combined with JEV phylogeny suggested that there are at least 5 genotypes of JEV under circulation[25] varying across the region as demarcated in Fig.3. While temperate areas tend to develop high epidemics during warm seasons, transmission in tropical regions peaks during rainy season. Most of the JEV-infected human cases are seen to be reported from tropical, sub-tropical and temperate regions of Asia, Australia with a recent case being identified from Angola, Africa[26,27]Prevalence of JEV is rising in India, Nepal, and other Southeast Asian countries, with recent cases reported in Pakistan, Papua New Guinea, and Australia, thus indicating towards an expansion in th geographic range[26]. Reportedly, long distance migrating water birds act as a vertebrate reservoir for the spread of JEV and its re-emergence from endemic tropical regions to temperate climate zones.

The most distinct strains of virus have been identified in Korea and Japan, spread over shorter distances by ducks[28,29]. Additionally, several avian species in North America can act as amplification hosts, as they are also susceptible to JEV infection[30] . This expansion in the geographical area of the disease/infection may have varied reasons like migration of birds, certain irrigation projects, smuggling of animals, and global warming.

2.3.2 Genome organisation and replication

JEV genome consists of a (+) sense RNA of around 11 kilobase (kb) which intertwines with multiple copies of the capsid protein to form the nucleocapsid of virus and is surrounded by host-derived phospholipid bilayer. An open reading frame (ORF) of JEV encodes for single polyprotein that consists of around 3400 amino acids and is flanked by 5' and 3' untranslated regions (UTRS) which form secondary structures to regulate RNA replication (as promoters and enhancers), transcription and translation during infection[16]. Cleaving of ORF by the host signalases and viral proteases yield three structural proteins (SP), namely capsid protein (C), membrane protein (M) and envelope protein (E) and seven NS proteins namely NS1, NS2A, NS2B, NS3, NS4A, NS4B, and NS5[15,18,31]. Functions for each structural proteins includes :-

- **Capsid Protein (C)** - Consists of 120 amino acids which form the homodimer formation and aid in the packaging of the viral genome and nucleocapsid [32].
- **Membrane protein (M)** - It has 75 amino acids and is formed in trans Golgi after the maturation and cleavage of the precursor to membrane (prM). prM is a 165 amino acid long glycoprotein with two transmembrane helices and helps in the assembly of the E protein[33].
- **Envelope protein (E)** - It is the primary target of neutralizing antibodies and forms the major structural component of the virion. It has a fusion peptide and a binding site for a cellular receptor[34].

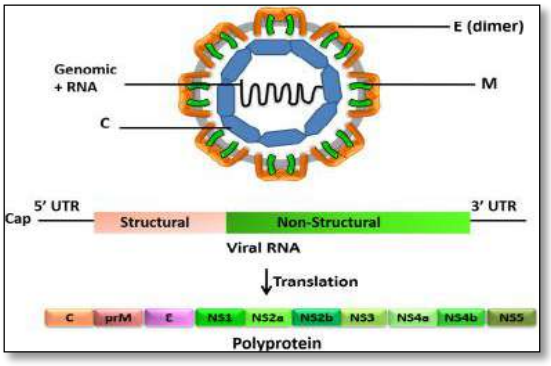

Fig 2.5. Representation of JEV structural and genomic organization

(Adapted from Sharma et al, 2021)

The seven non-structural proteins include:

- **Non-Structural Protein 1 (NS1)** - It is a 48 KDa protein which exists in homodimer formation i.e. in both secreted and cellular form, and is responsible for eliciting an antibody response in the host. Abnormal expression of JEV NS1 protein reported in persistent JEV infection[35].
- **Non-Structural Protein 2A (NS2A)** - This non-structural protein helps in recruiting viral RNA and all three structural proteins in viral RNA replication, assembly, and secretion towards the virus assembly site. It modulates the host antiviral response by inhibiting the interferon signaling pathway (IFN)[36].
- **Non-Structural Protein 2B (NS2B)** - It acts as co-factor for NS3 protease as it a forms a NS2B-NS3 heterodimer complex for proteolytic processing of the polyprotein, and also helps in the assembly of the replication complex by interacting with other NS proteins, along with NS3 anchoring in the ER membrane[37].
- **Non-Structural Protein 3 (NS3)** - NS3 is one of the largest and the most conserved protein as it has multiple enzymatic activities, making it a potential drug target. It has both RNA and protease helicase activities[38]. The N-terminal region of NS3, spanning around 179 amino acids, interacts with NS2B to cleave the precursor polyprotein into individual proteins[39]. The C terminus of NS3 behaves as an ATP-dependent RNA helicase, unwinding the double-stranded RNA genome during virus replication, hence catalysing the viral replication[40–42].
- **Non-Structural Protein 4A (NS-4A)** - Induces autophagy and mitophagy during viral replication and organizes the membrane-bound complex[43].
- **Non-Structural Protein 4B (NS-4B)** - Induces curvatures in the ER membrane forming distinct vesicle pockets where the replication complexes can sit and replicate the RNA genome, unidentified by host immune pathways[44].

- **Non-Structural Protein 5 (NS-5)** - Largest among all the proteins, consists of RNA-dependent RNA polymerase domain required for genome replication and capping of nascent RNA and methyl transferase activity[32].

On the cell surface, attachment factors help bind viral particles to a target cell. Next, receptor-mediated endocytosis is triggered by specific factors of the bound virion. Following internalization,the endosomal maturation pathway gets activated as the virion now passes from an early to the late endosome in a low pH. This acidic pH activates the viral E glycoprotein, causes the viral membrane to fuse with endosomal membranes. On release of viral RNA into the cytoplasm, it is translated into a polyprotein which is cleaved by viral proteases to further generate mature viral proteins essential for assembly and viral replication. Finally, the mature virions are released towards the extracellular side[45].

2.3.3 Neuroinvasive mechanism of JEV

JEV infected mice models show peripheral replication of virus and associated viremia along with distribution of brain lesions, strongly pointing towards the fact that JEV enters the CNS parenchyma through the blood. One of the critical features of the CNS is the Blood Brain Barrier (BBB), a highly selective, semi-permeable boundary made out of astrocytes, microglia, pericytes and mast cells.It forms a barrier between the peripheral circulation and the CNS thus protecting the brain from harmful pathogens like viruses and bacteria, from entering the CNS. The tight junction of the BBB is composed of certain proteins that are sensitive to inflammatory modulations and oxidative stress, such as claudin-5, zonula occludens (ZO)-1 and occludin present between the endothelial cells. JEV at a very high PFU in young mice breaches the BBB integrity as infection happens via intracerebral route and causes various neurological pathologies[45],[46]. JEV gains entry into the BBB via the following known mechanisms:

a) Transcellular infection of endothelial cells: To cross the BBB, neurotropic viruses are sometimes found to infect the endothelial cells. Images from electron microscopy of JEV infected cells depicted that endothelial cells can propagate infection to other supporting culture cells[47]. Cases of transcytosis have also been found in young suckling mice, where JEV particles move intracellularly across the endothelial cells in vesicles without disrupting the cell membrane[44].

b) Paracellular infection: By this mode of entry, JEV gains entry into the CNS using the increasing leakiness of the tight junctions between endothelial cells[48]. Breakdown of the tight junction proteins consisting of the Mast cells(MC) promotes BBB permeability by the action of MC-derived chymase causing mast cell degranulation. Thus MCs facilitate paracellular entry of JEV across BBB[45]. The BBB permeability also gets increased by the release of mediators like IL-6 (Interleukin-6), TNF (Tumor Necrosis Factor) and chemokines like -CCL5 (C-C motif chemokine ligand 5), CXCL10 (C-X-C motif chemokine ligand 10) etc.[49].

c) Trojan-Horse mode of entry: This theory of viral entry into the CNS is aided by the infection of the peripheral leukocyte cells as macrophages are majorly reported to be infiltrated in fatal JEV sample. Also, the damage of the endothelial barrier causes astrocytes and pericytes to release oxidative stress mediators like ROS (Reactive Oxygen Species) and MMP-9 (Matrix Metallopeptidase-9), which indirectly promote neuroinvasion[50].

2.3.4 JEV pathogenesis and clinical features

Pathogenesis due to JEV infection occurs in two phases, at peripheral tissues and in the CNS. Before entering and infecting the CNS, JEV primarily replicates in skin Langerhans cells (dendritic cells), from where it gets transported to the local lymph nodes, resulting in a lower viremia at the tissue site. As viral replication progresses after brief viremia, infected lymphocytes and monocytes cross BBB via endocytosis-, releasing mature virions into CNS. Inside CNS, JEV primarily replicates in neurons resulting in neuronal death via direct or

indirect neuronal killing. Direct killing of neurons involves JEV propagation inside neuronal cells and their ultimate death via apoptotic pathways and indirect killing causes neuronal death by inflammatory cytokines and reactive oxygen species produced by microglia.

Japanese Encephalitis Virus (JEV) is known to cross the placental barrier, posing a severe risk to fetal brain development and leading to neurodevelopmental abnormalities. Most JEV infections initially present with non-specific, flu-like symptoms including diarrhea, vomiting, rigors, abdominal discomfort, and upper respiratory features like coryza. This prodromal phase typically lasts between 5 to 15 days. While the majority of infections remain mild or subclinical, a small fraction (~1%) progress to acute encephalitic syndrome.

In Japanese Encephalitis (JE) survivors, long-term neurological complications are caused by neuronal cell death, impaired proliferation and arrested development of neuronal progenitor cells (NPCs) as a significant contributing factor. In severe cases, resting tremors, cogwheel rigidity, Bradykinesia and paralysis can occur with a mortality rate reaching up to 30%. Seizures are more frequently observed in children (85%) as compared to about 10% in adults. JE survivors frequently exhibit persistent neurological deficits, including movement disorders and cognitive impairments indicating viral-induced inflammation or damage to deep brain structures, particularly the thalamus and substantia nigra—regions critical for motor control.

Collectively, the clinical manifestations of JEV range from mild, nonspecific symptoms to severe neuroinflammatory syndromes with long-lasting consequences. Understanding these diverse neuropathological effects is crucial for managing JE survivors and guiding future therapeutic strategies.

2.3.5 JEV Diagnosis and Therapeutics

Various diagnostic tests are required to confirm the symptoms of impaired consciousness. To start with medication, we need to identify antibodies from natural infection or vaccination[51]. Various laboratory tests such as the Plaque reduction neutralization test, Nucleic acid

amplification, Testing CSF or serum for JEV-specific IgM antibodies can be done to essentially confirm the diagnosis of JEV.

Routine peripheral blood tests when performed showed non-specificities among JEV patients with reportings of either neutrophilia or hyponatremia. CSF of infected patients has lower probability of having mature virions than specific-lgM antibodies. Unlike other Flavivivirus, JEV is difficult to culture from human blood specimen, hence cannot be detected using the reverse transcription PCR (RT-PCR) assay. As no viral-specific transcripts gets detected in urine sample of infected patient, other available serological tests are done for diagnosing JEV, such as the hemagglutination inhibition (HI) test, IFA (Indirect immunofluorescence assay) and ELISA (Enzyme linked immune-sorbent Assay).

Given the severity of JE-associated outcomes with its ability to re-emerge in older and newer niches, there is a dire need for better diagnostics and precise JEV treatment. In such scenarios, it becomes essential to follow appropriate preventive measures. Seizures in JE-infected patients should be treated actively with routine sedation instead of corticosteroids or mannitol to improve disease outcome. Also, strong use of antibiotics should be avoided in JEV suspected patients to prevent antimicrobial resistance and further disruption of the body's natural fauna. Ribavirin, Interferon alpha2a, Dexamethosone, Igs and minocycline are known to successfully clear the clinical trials for JE treatment as they do not alter the disease outcome. At community levels we can organize various pest control programs to identify breeding mosquito niches and eliminate potential interactions between vectors and humans. Globally, governments can run vaccination campaigns, enhance children’s nutritional levels in high-risk endemic zones and conduct short-term immunization program in vector animals such as the pigs. While vaccination remains the most effective measure for controlling JE, preventing JEV infections remains an achievable goal.

2.4 The JaOArS982 Strain

The JaOArS982 strain is a well-characterized genotype III strain isolate of the Japanese encephalitis Virus (JEV) originated in Japan. As part of the Flaviviridae family, it shares genetic and structural characteristics typical of flaviviruses. Placed under the taxonomic category of *Orthoflavivirus japonicum*, highlighting its specificity among JEV strains[52].

2.5 Artesunate

Artesunate (Art) is a semisynthetic derivative of Artemisinin which is an endoperoxide sesquiterpene lactone compound, one of the active ingredients extracted from a Chinese medicinal plant *Artemisia annua*[53,54]. Art has a chemical formula[55] of $C_{24}H_{39}O_8$ and was discovered as a treatment against severe malaria owing to its exceptional efficacy against *Plasmodium falciparum and Plasmodium vivax.* Notable effectiveness of Art against multidrug-resistant Plasmodium strains, its high tolerance profile, and least adverse effects reflect its great pharmacokinetic and clinical value[54]. In addition to its antimalarial properties, recent studies have also shown anticancer, immune regulation, osteoporosis prevention, antiviral and antibacterial properties in experimentation with Art[56].

2.5.1 Synthesis- Industrially artesunate is produced by converting artemisinin to dihydroartemisinin (DHA) via semi-synthetic pathways using sodium borohydride in methanol. Acetylation of DHA with succinic anhydride in the presence of diisobutylaluminium hydride (DIBAL) yields artesunate. This therapeutic modification has introduced a hydrophilic group resulting in improved solubility and oral bioavailability[55].

2.6 Drug repurposing

First introduced by Ashburn and Thor, the term drug repurposing also known as drug repositioning, is the process of identifying new therapeutic uses for an already FDA-approved drug [57].This approach has gained significant attention due to its potential to reduce the time, cost and risk associated with traditional drug development.

Over the past decade, numerous successes, such as the use of zidovudine, initially marketed as an anti-cancer drug became the first anti-HIV drug to be approved by the FDA after intensive screening of *in vitro* compound libraries[58]. Also, remdesivir (initially developed for Ebola) got approved for its efficacy against COVID-19 out of the several other tested drugs such as the hydroxychloroquine and azithromycin. This incident emphasizes that leveraging known safety profiles of existing drugs can accelerate clinical trials and regulatory approvals, providing timely therapeutic options during pandemics. However, it also notes challenges such as limited efficacy in new indications and the need for robust clinical validation[59].

2.7 Artesunate derived Compound 9

Compound 9 (C9) is one of the prominently studied molecule at Dr. Ugir Hossain's laboratory within a series of synthesized artesunate-naphthalimide hybrid drugs designed for multimodal anticancer therapy[60]. C9 is a 4-azide-1,8-naphthalimide-artesunate conjugate, synthesized via an ester linkage. The synthesis involved converting 4-bromo-1,8-naphthalic anhydride into a hydroxyl-functionalized intermediate, which was subsequently azidated and conjugated with artesunate using EDC-HCl and DMAP. The compound was thoroughly characterized using Nuclear Magnetic Resonance (NMR) spectroscopy, LCMS(Liquid chromatography–mass spectrometry) and HR-MS(High-Resolution Mass Spectroscopy), confirming its structural identity.

Biologically, C9 demonstrated strong DNA intercalating properties, as reported by UV-visible and fluorescence spectroscopy studies. Upon binding to salmon testes DNA, it exhibited a prominent red shift in absorbance from 367 nm to 376 nm, along with hypochromicity, indicating effective intercalation. The compound also caused a decrease in fluorescence intensity upon increasing DNA concentration, supporting its DNA-binding ability. In competitive dye displacement assays, C9 displaced ethidium bromide and acridine orange, further affirming intercalation, while its effect on Hoechst 33342 suggested minimal groove

binding. This intercalating viral DNA or RNA induces oxidative stress which can damage viral proteins and nucleic acids, interfering with replication and transcription.

2.7.1 Synthesis **-** The compound 9 drug is synthesized by a multistep process - Initially, 4-bromo-1,8-naphthalic anhydride is reacted with 2-aminoethanol to form an intermediate, which is later modified with sodium azide to introduce the azide functional group. In an inert environment, this azide-substituted naphthalimide is subsequently coupled with Art using EDC.HCL (1-Ethyl-3-(3 dimethylaminopropyl carbodiimide hydrochloride) and DMAP (4-Dimethylaminopyridine) as coupling agents. Column chromatography is used to purify the finished product, and to confirm its structure and purity, characterization methods such as NMR and HR-MS are used[60] (Fig-1.6). Compared to similar compounds synthesized by Hossain et al., such as compounds 3, 5, and 7; compound 9 demonstrates superior efficacy. Its DNA intercalation is stronger, as evidenced by greater binding constants and notable redshifts in spectroscopic studies. This enhanced interaction is due to the azide substitution, which also increases the compound's reactivity and effectiveness. Compound 9 shows greater activity in reducing cell viability and controlling tumor growth. Its ability to combine DNA interaction with oxidative stress induction and apoptosis activation makes it more robust and versatile than its counterparts. Compound 9's unique structural and functional properties are both a powerful anticancer agent and also opens avenues for its application in antiviral therapies. Its dual-action mechanism ensures a broad spectrum of activity, offering promising potential for further clinical development.

2.7.2 C9 as a treatment for JE

Naphthalimide (1H-benzo[de]isoquinoline-1,3-(2H)-diones) and its derivatives, especially naphthalene diimides (NDIs), have gained significant attention in drug development over the decades. Due to their highly planar, π-deficient, aromatic or heteroaromatic core which facilitates DNA intercalation and nucleic acid targeting, these compounds can exhibit broad

range of applications ranging from their use as fluroscent dyes and sensors or as local anesthetics[61], analgesic[62], antitrypanosomal[63] to even cancer therapeutics and antiviral agents. Early antiviral efforts with naphthalimide derivatives focused on simple 2-amino-naphthalimide analogues, which exhibited modest antiviral activity against herpes simplex viruses (HSV-1 AND HSV-2)[64]. In this study, compounds 14–16 demonstrated EC_{50} values ranging between 16–20 μg/mL for HSV-1 and 56–72 μg/mL for HSV-2. Although less potent than standard antiviral agents like acyclovir, this initial study confirmed the naphthalimide scaffold's viability for antiviral modification which later advanced considerably with the development of core-extended NDIs targeting HSV-1. In a 2015 landmark study by Perrone et al., researchers synthesized NDIs that specifically bind to G-Quadruplex structures which are four-stranded secondary structures present in both host and viral genomes and thus effectively blocking the viral gene transcription. These NDI derived compounds showed low-nanomolar inhibition towards two strains of HIV-1 replication, highlighting the power of structural design in modulating antiviral efficacy[65].

Some naphthalimides are linked to other functional drugs (e.g., artesunate[60], CXCR4 inhibitors[66]) using ester or amide bonds forming a dual-action design i.e. the molecule interacts with the viral DNA to shut down transcription and blocks the host receptor interaction to prevent viral entry.This synergistic mechanism represented a promising new direction in antiviral design as these hybrid naphthalimide-based molecules act through both DNA-targeted and receptor-level mechanisms. Structural modifications such as core extension, functional conjugation, and metal complexation significantly enhanced their selectivity and potency, making them promising leads against various complex viruses. Taken together, these studies established naphthalimides and NDIs as versatile antiviral scaffolds capable of targeting both viral genomes and host-pathogen interaction points, thus hinting the role of Compound 9 (C9) for antiviral therapy.

Chapter 3

AIM OF THE STUDY

The primary aim of this study is to explore the therapeutic potential of Artesunate and its derivative compound 9 against Japanese Encephalitis Virus (JEV) Infection in HT22, a mammalian neuronal cell line and further test its efficiency in murine model.

OBJECTIVE 1: To investigate the cytotoxic profile of Artesunate and Compound 9

OBJECTIVE 2: To evaluate and compare the antiviral efficacy of Artesunate and its derivative C9 against Japanese Encephalitis Virus infection.

OBJECTIVE 3: To investigate the effect of Artesunate and Compound 9 on survival in JEV infected BALB/c mice.

Chapter 4

MATERIALS AND METHODS

4.1. Ethics Statement, Virus Propagation and Plaque Assay

Approval for all the animal experiments was received from the Institutional Animal and Ethics Committee (IAEC), National Brain Research Centre (Approval no. NBRC/IAECI2017/128). BALB/c mice pups were housed together with their mothers under a 12-hour dark/ 12 hour light cycle at constant temperature and humidity with food and water ad libitum as defined by the CPCSEA (Committee for the Purpose of Control and Supervision of Experiments on Animals, Ministry of Environment and Forestry, Government of India). Japanese Encephalitis Virus strain JaOArS982 is used for infection and propagation in suckling P2 BALB/c mice. Brain was harvested after observing terminal illness symptoms. A 10% tissue suspension was made to homogenize in serum-free DMEM and further centrifuged at 15,000xg for 50 minutes to separate the tissue debris. Viral supernatant obtained was filtered through a 0.22 µm sterile filter and stored in smaller aliquots at -80ºC. Virus titre was determined by plaque formation on porcine stable kidney cells (PS) monolayers.

For plaque assay, six well plates were seeded with 2×10^5 PS cells in 10% DMEM which when at 70% confluency was replaced with serum-free DMEM for 2 hours. The cells were then inoculated with 10-fold serial dilutions of virus (10^{-3} to 10^{-9}) for infection and again incubated for 2 hours at 37°C. The inoculum was removed and cells were gently washed with PBS. A 3 ml agarose overlay medium (2X incomplete MEM, 5% FBS, 2% low melting agarose, and 1% penicillin-streptomycin) was poured into each well. The plates were incubated at 37°C for 72-96 hours and were then fixed with l0% PFA for 4 hours at room temperature and overlay was removed before staining with crystal violet to visualize and count plaques.

4.2. Artesunate and Compound-9 (C9)

Artesunate(A2191, TCI Shanghai) and Compound-9 (C9)[60] were received as a kind gift from Dr. Ugir Hossain (Chittaranjan National Cancer Institute, Kolkata). The molecular weight of Artesunate is 384.43 g/mol and, that of C9 is 648.66 g/mol. Stocks for both the compounds were prepared in DMSO and, aliquots were stored at -30ºC. At the time of experiment, aliquots were used to prepare the required drug concentration in DMEM.

4.3. Cell Line and Cell Culture

HT22, an immortalized mouse hippocampal neuron cell line, gift from Shiv K. Sharma (NBRC,India), and Porcine stable kidney cells (PS cells), a kind gift from Dr. Manjula Kalia (Regional Centre for Biotechnology, Faridabad, India) were cultured in DMEM (HT22) and 1X MEM (PS), both supplemented with 10% heat-inactivated fetal bovine serum (FBS), penicillin (100 units/ml) and streptomycin (100 µg/ml) in 5% CO_2 incubator at 37ºC with relative humidity of 60-80%. All the reagents for cell culture were obtained from Gibco, unless stated otherwise.

4.3.1 Cell Thawing

Water bath is pre-maintained at 37°C so that frozen vials could be taken out from liquid nitrogen and thawed quickly. The cell suspension was added to a falcon containing fresh media (10% FBS DMEM/MEM) and centrifuged at 720-750 rpm for 3 minutes. The pellet was re-suspended in 1 ml of fresh media and seeded with 8 ml of fresh media in a T75 flask. The flask was maintained at ambient conditions till the optimum confluency for splitting was achieved.

4.3.2 Cell Freezing

Upon 70% confluency (log phase), cells were washed with 1X PBS and trypsinized for 2 minutes in incubator. Once detached, the trypsin solution was neutralized using double volume of pre-containing media and whole media was collected in a fresh 15ml falcon tube and centrifuged. The pellet was re-suspended in freezing mixture containing 90% FBS & 10%

DMSO and stored at -80°C in CoolCell cryobox for reducing the temperature @2ºC/min. For long term storage the vials were stored in liquid nitrogen after 1 day storage in -80°C freezer.

4.3.3 Cell counting and infection

Upon reaching 70% confluency, cell seeded plates were switched to serum free DMEM, 2 hr. prior to virus inoculation. Meanwhile, cell count was performed by pelleting down the cells and mixing 20 µl of each - cell suspension and trypan blue. 10µl each of this suspension was charged into both of the Neubauer chamber and count was done against bright field cell counter. Final cell count was calculated by taking the average no. of live cells in both the chambers. For experiments, cells were infected at Multiplicity of infection (MOI) 3 of JEV JaOArS982 strain for 2 h, followed by sterile PBS wash to remove any non-internalized virus. Monolayers were then maintained in1% FBS containing DMEM and cells were harvested at 24-hour post infection.

4.3.4 Treatment paradigm for Artesunate and Compound-9

HT22 cells were harvested from a T-75 flask and were made to grow in a 6-well plate at a seeding density of $0.3*10^6$ for about 12 hours. For each compound six conditions were maintained including 1) Mock cells, 2) Only treatment controls for each drug at both 0.1 µM and 0.3 µM concentration, 3)only JEV infected cells, 4)JEV infected cells with treatment at 0.1 µM and 0.3 µM concentration. At around 70% cell confluency, serum free DMEM was added to cell plate for 2 hours after which cells were infected with JEV JaOArS982 strain at MOI 3 for 2 hours. Art and C9 treatment (each at 0.1µM and 0.3µM) was prepared meanwhile from stock in 1% FBS-DMEM and cells were then incubated for 24 hours following which cell plates were washed with 1X PBS and collected for further analysis at -30ºC.

4.4. RNA extraction and further processing

4.4.1 RNA Isolation

Total cellular RNA was isolated from cells using 200 µl of RNAiso Plus (TAKARA BIO INC.) for cell lysis. Further, phase separation was done using 40 µl of chloroform (1/5th of Trizol) followed by incubation at RT for 5-10 minutes and centrifugation at 12000 rpm for 15 minutes. Next, top aqueous layer containing RNA is obtained in a fresh tube and treated with 200µl isopropanol to precipitate RNA. After 15 minutes incubation at RT, tubes were again centrifuged at 12000 rpm for 15 minutes. The supernatant was carefully decanted without disturbing the pellet. Precipitated RNA pellet was washed twice by adding 200 µl of 70% ethanol and centrifugating at 7500 rpm for 10 minutes so that any extra salts get dissolved in it and RNA remains intact at the bottom. The pellet is then air-dried in laminar hood and re-suspended in 20 µl RNase free water.

4.4.2 cDNA Preparation

Briefly, cDNA (5ng/µl) was synthesized using Verso cDNA synthesis kit (Thermo Fisher, USA). Each reaction consisted of RNA, RNase free water and master mix. Following cocktail of master mix (7µl) was used per reaction:

Component	Volume (µl/reaction)
5x cDNA synthesis buffer	4µl
dNTP mix	1µl
Random Hexamers	0.75 µl
Anchored Oligo dT	0.25 µl
RT enhancer	0.5µl
Verso Enzyme mix	0.5µl

Thermal cycling conditions were set as follows:

	Temperature	Time	No. of Cycles
cDNA synthesis	42°C	30 minutes	1
Enzyme inactivation	95°C	2 minutes	

4.4.3 qRT-PCR

Quantitative real time PCRs(qRT-PCRs) were performed using SYBR green PCR Master Mix (BIORAD) for gene specific primer sequences (JaOAr and GAPDH) as mentioned in Table 2. The reaction mixture for 1 reaction was made as follows:

Component	Volume
SYBR Green	5µl
RNAse Free Water	2µl
Forward primer	0.5µl
Reverse primer	0.5µl

The below mentioned thermal cycling conditions were use

	Temperature	Time	No. of cycles
Denaturation	95°C	60 seconds	1
Denaturation	95°C	30 seconds	40
Annealing	58ºC	30 seconds	
Extension	72°C	40 seconds	
Final extension	72°C	180 seconds	1

Relative gene abundance for each reaction was determined using delta Ct method with GAPDH as loading control in ViA 7 Real-Time PCR System (Applied Biosystem) where threshold cycle values were determined using the software of the instrument. Results were expressed as fold differences between mock and viruş infected samples.

4.5. Immunoblotting

Whole cell protein extract was prepared using complete lysis buffer and the protein obtained was estimates using BCA agent. The required concentration of protein sample was separated and target proteins were visualized via western blotting.

4.5.1 Protein Isolation

Incomplete Lysis Buffer was prepared as mentioned in Table 3. Later, sodium-orthovanadate (4 µl SOV/ml) and protease inhibitor cocktail (2ul PIC/ml) was added to make the complete lysis buffer.For isolation, plates were kept on ice for 10 minutes. Cells were washed with complete lysis buffer and the cell suspension obtained was sonicated twice for 10 pulses using Ultrasonic Homogeniser (Biologics, Inc.) to lyse the cells. Sonicated samples were centrifuged for 50 minutes at 12,000 rpm at 4ºC. The supernatant obtained was collected and stored at -30°C.

4.5.2 Protein Estimation

The quantity of protein in the obtained supernatant was estimated using bicinchoninic acid solution or BCA reagent (Sigma, USA) which works similar to Lowry procedure. As both of the procedures require alkali medium and lead to the formation of a Cu^{2+}-protein complex followed by the propotional reduction of Cu^{2+} to Cu^{1+} by the protein amount present in the sample. The first step of this reaction follows the biuret reaction wherein a light blue complex is formed from the chelation of copper with protein in an alkaline environment. Peptide proteins with three or more amino acid residues majorly (cysteine or cystine, tyrosine, and tryptophan) form a coloured chelate complex with cupric ions in an alkaline environment containing sodium potassium tartrate.

In the second step, highly sensitive detection of the now reduced cuprous cations (Cu^{1+}) is done by BCA. As two molecules of BCA chelate with one cuprous ion to develop the intense purple-

colored, water-soluble BCA/copper complex and exhibits a strong linear absorbance at 562 nm with increasing protein concentrations.

4.5.3 SDS-PAGE

Equal amount of each protein sample was mixed with the loading dye in a 9:1 and boiled in water bath for 5 minutes and cooled at room temperature prior to gel loading along with the molecular weight ladder.

a) Principle behind SDS PAGE:

Polyacrylamide gel electrophoresis (PAGE) is the most common technique that is used to separate and characterize proteins. Acrylamide alone forms linear polymers, bisacrylamide introduces crosslinks between polyacrylamide chains. The pore size is decidedby the concent ration of acrylamide and bis-acrylamide. A high ratio of bisacrylamide to acrylamide causes smaller pore formation and thus lower electrophoretic mobility. The size of the pores created in the gel is inversely related to the amount of acrylamide used. Gels with a lower percentage of acrylamide are used to resolve large proteins and high percentage gels are used to resolve small proteins.

b) Chemical components used in SDS-PAGE:

1. Acrylamide: It is a white crystalline powder that auto-polymerizes upon dissolving in water. Activated monomers in their free radical state polymerize to form long chain polvmers. As these chains keep sliding over one another solution of these chains is viscous but does not form a gel.

2. Bisacrylamide: N, N''-Methylene bisacrylamide is the cross-linking agent for Acrylamide chains. Acrylamide and bisacrylamide are used in a ratio of 29:1. 29gm Acrylamide and 1 gm bisacrylamide are weighed and dissolved in 80 ml water. The volume is made up to 100 ml and the solution is stored at 4°C in dark as it is light sensitive.

3. SDS: Protein mix when heated at 100ºC in the presence of SDS, forms individual polypeptides by denaturing the proteins. All proteins, therefore carry an overall net negative charge per unit length as SDS wraps around the polypeptide backbone and negates the intrinsic polypeptide charges in comparison to the overall charge. Hence, proteins are separated on the basis of molecular weight alone.

4. Tris: Having a pKa of 8.3 at 20ºC, Tris acts as the buffer solution.

5. APS: Ammonium per sulphate or APS causes spontaneous decomposition of free radicals upon catalyzation by the TEMED thus initiating the gel formation.

6. TEMED: N,N,N'',N'' tetramethylethylenediamine is added at the end while preparing gel. It reacts with APS to split persulfate ions into sulfate free radicals. These free radicals now initiate the polymerization (free radical reaction) of the acrylamide and cross-linking with bisacrylamide. If the concentration of APS and TEMED is increased, it would result in decreased average polymer chain length and gel elasticity while increasing the gel turbidity. Decreasing the initiators amount would reverse the effect.

7. Glycine: The non-uniform charge and pH of glycine in stacking and resolving gel sets the basis for electrophoretic stacking and protein separation. pH of stacking gel (6.8, pKa 2.45) is maintained above and for resolving gel pH (8.8, pKa 9.6) is set below the pI of gly (5.97). Therefore in stacking gel, glycine predominates as glycine zwitterions which has no charge. Continuous current allows the gel to run while the anionic protein species carry the charge in place of zwitterions. This allows the protein to stack in a thin band behind the highly mobile chloride ions as glycine is present in between the protein molecules which constrains the separation of proteins. Entry into the resolving gel presents the protein band with both pH increase (basic pH 8.8) and a pore size decrease. As zwitterions deprotonate to their anionic form, the amount of charge carried by the proteins decreases and the movement of proteins is no longer constrained. Hence, proteins within the resolving gel separate based on molecular weight.

8. Bromo Phenol Blue: BPB is a small, negatively charged, ionizable molecule used as marker dye. As proteins and nucleic acids are mostly colourless, it becomes essential to mark them with a dye lest they run off the gel during electrophoresis. Use of BPB as a tracking dye allows to visualize proteins and nucleic acids as it weakly binds with them to give blue color and also stays ahead of them (owing to its smaller size).

c) Gel Preparation :

10% resolving Gel was first prepared according to table 6 in appendices and poured into Bio-Rad gel mould (Bio-Rad, CA, USA) consisting of two glass plates clamped together with 1.5 mm spacers on either side. The plates were clamped onto the stand and the resolving gel solution was poured. After pouring, the gel was layered with methanol to avoid bubble formation and allowed to polymerize at RT for 15-20 min. After polymerization the methanol was drained off just before adding the stacking gel. Meanwhile contents for the 4% stacking gel (mentioned in table 7, appendices) were prepared and mixed gently in a 15 ml falcon. The stacking gel solution was poured over the resolving gel. The comb (1.5 mm deep well: BioRad) was placed into the solution and the gel was allowed to polymerize for 15-20 min.

d) Sample Preparation:

Amount of protein sample to be loaded was aliquoted in a separate eppendorf tube. Loading dye(stacking gel buffer, glycerol, 10% SDS, 0.5% Bromo-Phenol Blue and β-ME in water) was kept at 95°C in dry bath for 5 min. 1 part of this dye was added to 9 parts of the protein sample to make the final concentration of 1µg of protein/µl for all samples. The samples were then heated in the dry bath for 5 min at 95°C and cooled to RT. Meanwhile gel molds were put Into the electrophoresis tank containing 1X electrode buffer. The gel comb was removed and Rainbow marker solution for protein molecular weight was used as a ladder after which samples were sequentially loaded into the wells.

4.5.4 Western blotting protocol

Gel electrophoresis was used for protein separation at a constant voltage of 150V and starting current of 55-60 mA for each gel until the blue dye front reached the bottom of the gel, the separated proteins are transferred onto a nitrocellulose membrane which is kept towards anode and sandwiched with the gel (towards cathode) between foam pads that are submerged in ice-cold 1X transfer buffer. An electric field of constant Voltage (90V) is applied for 90 minutes. The proteins move out of the gel and get tightly attached to the membrane surface, yielding a copy of the gel protein on membrane which is checked using Ponceau dye. After transfer, the membrane was blocked using 10% skimmed milk in TBST for three hours under gentle shaking conditions to prevent non-specific binding of the antibody to the membrane surface. The transferred protein is then probed sequentially with primary antibody diluted in TBST-BSA at 4°C overnight with gentle shaking.Dilution used for antibodies are enlisted in table 1. Next day, 5 TBST washes were given at RT for 5 minutes each. HRP-conjugated secondary antibody (goat-anti rabbit,Vector Laboratories, USA) was added at a dilution of 1:7500 for 1.5 hours to detect the localized probe to document the location and relative abundance of the target protein. Blots were again washed 5 times for 5 minutes each with TBST before developing them in Immobilon western chemiluminescent HRP substrate (Millipore, Sigma) in Uvitec Cambridge (Cleaver Scietific, UK).

4.6. Cell Titre Blue Viability assay

The viability of cultured cells was determined using CellTiter-Blue Reagent (Promega) which in living cells reduce resazurin (has ability to penetrate cells) to resorufin (fluorescent, can diffuse out of cells) by the action of mitochondrial, cytosolic or microsomal enzymes. HT22 cells were seeded at a density of $10*10^3$ cells per well in a 96-well plate. At around 30% confluency, cells were serum deprived for 2 hours and various drug doses were added in triplicates to be kept in incubation for 24 hr. Next day, 12µl of Cell Titer-Blue Reagent

was added to each well followed by 3 hr. of incubation in dark at 37ºC in 5% CO_2 incubator. Absorbance was recorded at 573nm using Glomax Explorer (Promega).

Results were expressed as relative percentage of viable cells in different drug concentrations to that of the viability in mock cells. The 50% cytotoxic concentration (CC_{50}) was calculated by the nonlinear regression (curve fit) in GraphPad Prism9 (version 9.5.1) software.

4.7. Immunocytochemistry

Briefly, HT22 cells were grown in 8-chambered permanox slides followed by JEV infection at 3MOI. Post infection, cells were fixed with 4% paraformaldehyde solution for 20 minutes and permeabilized with 0.5% PBXT followed by blocking with 5% BSA (Sigma, USA) + 5% goat serum (prepared in 0.01% PBXT) for 1 hour. Cells were then incubated in a humid chamber overnight with Primary antibodies: NS3 (1:500, Genetex) at 4ºC, followed by brief period of eight PBXT washes. Cells were next incubated with appropriately tagged secondary antibody Alexa Fluor 594 (anti-mouse, raised in goat, utilizing 1:2500 in PBS) and were mounted with DAPI (Vector Laboratories, USA). Images were captured on Zeiss Apotome microscope (Carl Zeiss, Germany) at 20X magnification. NS3 positive cells were then manually counted for all the conditions.

4.8. Nitric oxide (NO) assay

Nitric oxide released from cultured cells following JEV infection was assessed using Griess reagent (Sigma, St. Louis, USA). In a 96-well plate, 100 µL of Griess reagent was added to 100 µL of cell supernatant obtained at the time of 6-well plate collection of mock, infected and treated cells. This plate is then left in dark for 15 minutes incubation time. The intensity of the color developed is proportional to the amount of nitrite accumulated which was estimated at 540nm with the help of Multiskan SKY Spectrophotometer (Thermofisher Scientific). The relative amount of NO release was plotted by calculating the mean fluorescence intensity recorded.

4.9. Annexin-Propidium Iodide staining

AnnexinA5 or annexinV (ANXV) is a phospholipid-binding protein with high affinity for phosphatidylserine which in healthy cells is located on the outer leaflet (extracellular side) of the plasma membrane. During apoptosis, phosphatidylserine translocates itself from the inner to the outer cytoplasmic surface of the plasma membrane and this externalization of phosphatidylserine forms the basis of Annexin-PI staining. Hence, living cells are Ann V negative and propidium iodide (PI) negative, early apoptotic cells are Ann V positive but PI negative, living cells with a disturbed membrane are ANXV negative but PI positive whereas late apoptosis or necrotic cells are both Ann V and PI positive. FITC Annexin V Apoptosis Detection Kit I (BD Pharmingen) was used to determine the cell death in uninfected control, JEV-infected and treated HT22 cells. After 24 hr. treatment paradigm, cells were trypsinized from 6-well plate and the pellet obtained was washed twice with 1X PBS mediated by centrifugation at 500-600 rpm for about 1 min. Pellet was then resuspended in 1ml (for 10^6 cells) of 1× binding buffer (25mM HEPES plus NaOH, pH 7.4, 140mM NaCl and 1mM CaCl2). Then, 100µL of each sample (1×105 cells) was incubated with 5µL each of FITC-labeled ANXV and PI. All samples were then vortexed slightly before incubating in the dark for 15 min at RT. After 15 minutes, 400µL of binding buffer was added to each sample which was analyzed in BDFACS Verse (BD Biosciences, USA) using FCAP Array 3.0 analysis software. After selecting cell clusters for required cell death evaluation by flow cytometry, initial gating was done using an unstained control (without ANXV or PI). The relative percentage of cells which double-stained for both Ann V and PI were represented in the plot.

4.10. Measurement of reactive oxygen species (ROS)

Reactive oxygen species (ROS) are inevitable by-products of aerobic cellular metabolism and play important role in intracellular cell signaling as their levels increase dramatically under cellular oxidative-stress. To detect its generation in cell culture, non-polar H2O2 sensitive dye

5-(and-6)-chloromethyl-2′7′-dichlorodihydrofluorescein diacetate (CM-H2DCFDA) (Sigma Aldrich) was used as an indicator. It is a nonfluorescent, cell-permeable, chemically reduced form of fluorescein which upon cleavage of the acetate groups by intracellular esterases are converted to the highly fluorescent 2',7'-dichlorofluorescein (DCF).For measuring ROS levels, HT22 cells were seeded in a 96 well black/clear-bottom plate and the treatment paradigm was followed as stated above. At 24 hpi, pre-media was removed and cells were then washed with 1x PBS. 25 μM DCFDA was prepared from 10 mM DCFDA stock (in DMSO) and added to wells in Serum Free DMEM prepared without phenol red. The cells were then incubated for 45 min in dark after which DCFDA containing media was removed and the fluorescence intensity reading was taken in just the serum free DMEM at 485 nm/535 nm using Glomax Explorer (Promega).

4.11. Murine infection and *in vivo* experimental paradigm

For all *in vivo* experiments performed to compare the therapeutic effects of Artesunate and C9, post-natal day 10 BALB/c (Bagg Albino) mice pups were randomly selected without any sexual bias and divided into 4 groups: Mock, JEV-infected (JEV), only treatment (Art/C9), JEV-infected and treated (JEV+ Art/C9). At Day 0, all pups to be infected were intraperitoneally given $3x10^4$ plaque-forming units (PFU) of JEV JaOArS982 strain. Mock group received an equal volume of phosphate-buffered saline (PBS). After 24 hours, treatment was administered in PBS intraperitoneally at a dose of 3mg/kg, 7mg/kg and 10mg/kg in only treatment (ART/C9) and JEV+ART/C9 group for six consecutive days. Meanwhile, JEV groups were injected with equal volumes of DMSO. From 5^{th}-6th day onwards, JE symptoms started to show up in animals which included restriction of movements, poor pain response, piloerection and hind limb paralysis. All the animals were sacrificed either when terminally ill symptoms appeared, referred to as full symptom (FS) or on 30^{th} day post infection (dpi) indicating complete survival.

4.12. Statistical Analysis and Graphical illustrations

Data were represented as mean ± SD of three independent experiments unless otherwise stated. GraphPad Prism9 (version 9.5.1) was used for data analysis and preparations of graphs. Significance within all selected drug concentrations of both the compounds were analyzed using one-way ANOVA with Tukey post hoc test to compare control with infected and treated samples. Two tailed Student's t-test or two-way ANOVA was used to check the significance between two independent groups. Any p-value less than 0.05 was considered as statistically significant.

All the graphical illustrations were prepared using BIORENDER.org

Chapter 5

RESULTS

5.1 Synthesis of Compound-9(C9)

The structure of the synthesized artesunate-naphthalimide conjugate (Compound 9) was confirmed by thoroughly done ^{1}H-NMR spectroscopy at Dr. Ugir's lab. The spectrum was recorded using a Bruker Avance-III 400 MHz spectrometer in DMSO-d_6 or $CDCl_3$ solvent and the values for the Chemical shift and coupling constant (*J*) were reported in ppm(δ) and hertz (Hz) respectively.

Characteristic aromatic proton signals of the naphthalimide moiety in intermediate compound 1 synthesized by reacting 4-bromo-1,8-naphthalic anhydride with ethanolamine were confirmed by its appearance as multiplets in the downfield region: δ 8.50 (dd, J = 7.3, 1.2 Hz, 1H), 8.44 (d, J = 8.0 Hz, 1H), 8.37 (dd, J = 8.4, 1.2 Hz, 1H), 7.83 (dd, J = 8.5, 7.3 Hz, 1H), and 7.70 (d, J = 8.1 Hz, 1H), indicating successful retention of the DNA intercalating core.

A singlet at δ4.81 ppm corresponded to the amide proton, while the aliphatic region showed triplets at δ 4.14 and 3.63 ppm, representing the ethylene protons of the ethanolamine side chain. In intermediate Compound 2, formed by azidation of Compound 1, the aromatic protons remained largely unchanged with peaks at δ 8.47, 8.40, 8.34, 7.81, and 7.68 ppm, indicating preservation of the core structure. The linker methylene protons also appeared at δ 4.12 and 3.62 ppm, suggesting successful conversion of the terminal hydroxyl to azide without disrupting the backbone.

In intermediate Compound 3, which involved coupling of artesunate with Compound 2 via EDC/DMAP chemistry, the aromatic signals of the naphthalimide ring were retained (δ 8.50 to 7.70 ppm), while new signals appeared in the aliphatic region: δ 5.55–5.44 (m, 2H) and δ 4.38–4.26 (m, 4H), attributed to the artesunate moiety. Multiple methyl and methylene signals between δ 2.59 and 0.62 ppm confirmed the presence of the artesunate framework. The final structure of Compound 9 was thus confirmed through the combined presence of aromatic

signals from the DNA-intercalating naphthalimide, and the aliphatic region consistent with artesunate, verifying successful conjugation through the designed synthetic route.

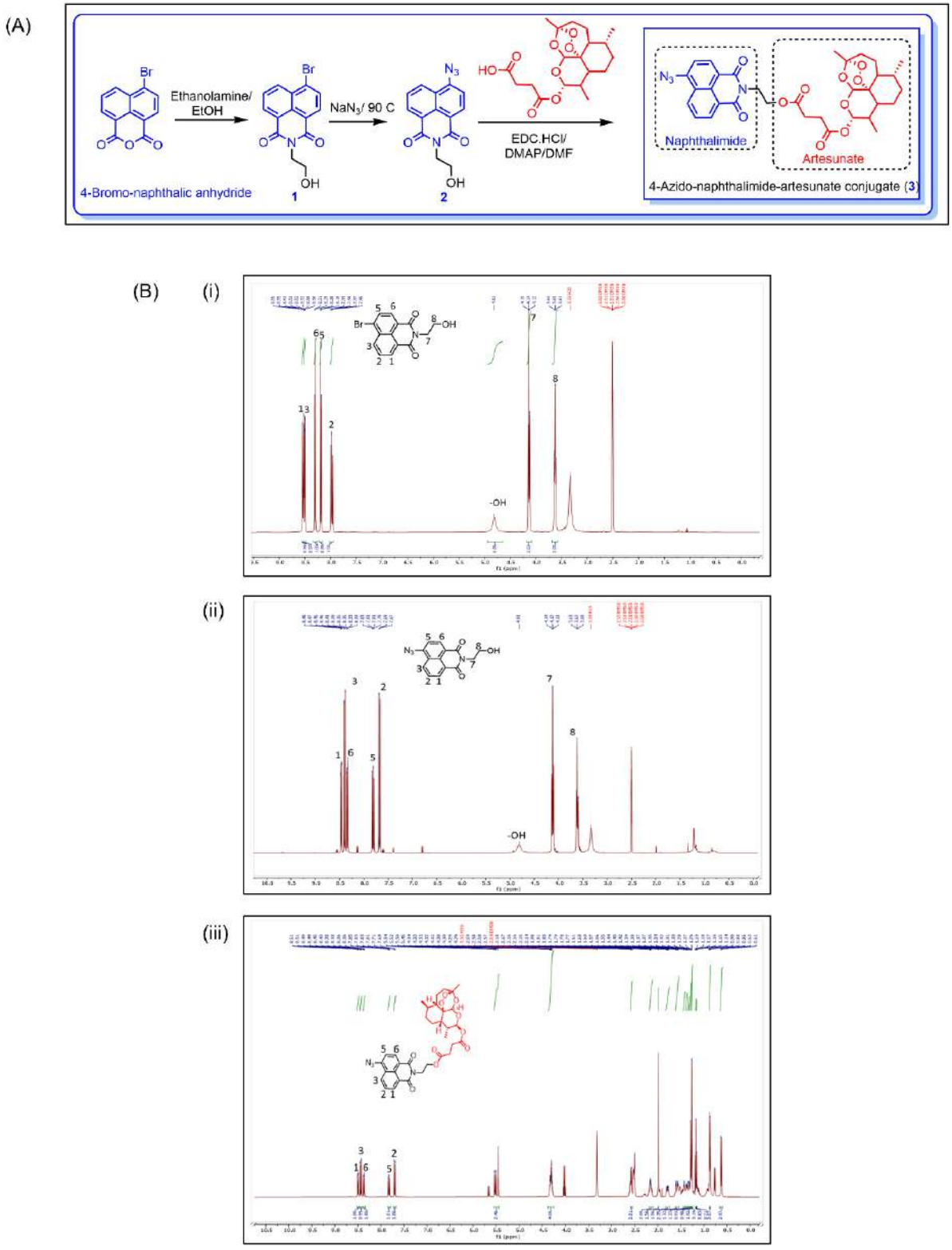

Fig 5.1. Structural conformation of compound 9 by ^{1}H-NMR wherein (A) represents the overall chemical synthesis of C9 and (B) showing the NMR data of its intermediate Compound1 B(i), Compound 2 B(ii), Compound3 B(iii).

5.2 Evaluating cytotoxic profile of Artesunate and Compound-9

5.2.1 Analysing Cell Viability of Artesunate and Compound-9

Cell viability assay was performed using Cell Titer Blue Reagent to assess the cytotoxic effects of Artesunate and Compound-9. HT22 cells were seeded in a 96-well and incubated with various drug concentrations ranging from 0.1 µM to 150 µM for 24 hrs. Post treatment, the relative percentage of viable cells was plotted as in Fig 5.2(a) wherein both Artesunate (purple bars) and Compound-9 (orange bars) demonstrated a concentration-dependent reduction in cell viability compared to Mock (untreated cells) (0 µM). At lower concentrations (0.1–0.5 µM), both the compounds maintained >80% cell viability while C9 significantly showed >=100% cell viability at these concentrations (0.1–1µM). Artesunate exhibited a stronger cytotoxic effect from 1 µM onwards, resulting in significant decline in viability at comparable doses. At higher concentrations (10–28 µM), viability dropped below 40% for both compounds, and 150 µM was observed to be highly cytotoxic for both compounds similar to the 10% DMSO wherein 90% cytotoxicity was evident.

Notably, the CC_{50} values were calculated using nonlinear regression in GraphPad Prism9 software. Artesunate (CC_{50} = 9.69 µM) showed a higher cytotoxic potency than C9 (CC_{50} = 20.99 µM), as seen in Fig 5.2(b). This figure also illustrates the dose-dependent increase in the percentage of dead cells for both compounds. Artesunate showed a steeper increase in cell death as compared to Compound-9 which showed a trend uniform to its lower CC_{50} value.

5.2.2 Comparing morphological effects of Artesunate and Compound-9 on HT22 cells at selected drug concentrations

As 0.1 µM and 0.3 µM of each compound showed significantly higher percentage of viable cells as compared to the rest, both of these drug concentrations were considered for upcoming

further experiments. Before proceeding, morphological effects of both of these drug concentrations were assessed for each Artesunate and C9. Phase-contrast images of HT22 cells were taken at 20X magnification for the treated cells (both concentrations) and compared with mock cells. The treated cells exhibited no apparent morphological differences compared to the untreated cells. Cells across all groups, including mock cells had well-adhered monolayers of cell population exhibiting the perfectly inter-connected network of typical spindle-shaped HT22 cells with intact cellular structures and no signs of cellular stress were observed. These observations suggest that at lower concentrations (0.1 μM and 0.3 μM), both Artesunate and Compound-9 have maintained the healthy cell morphology also supporting the results from cell viability assay observed before for these concentrations.

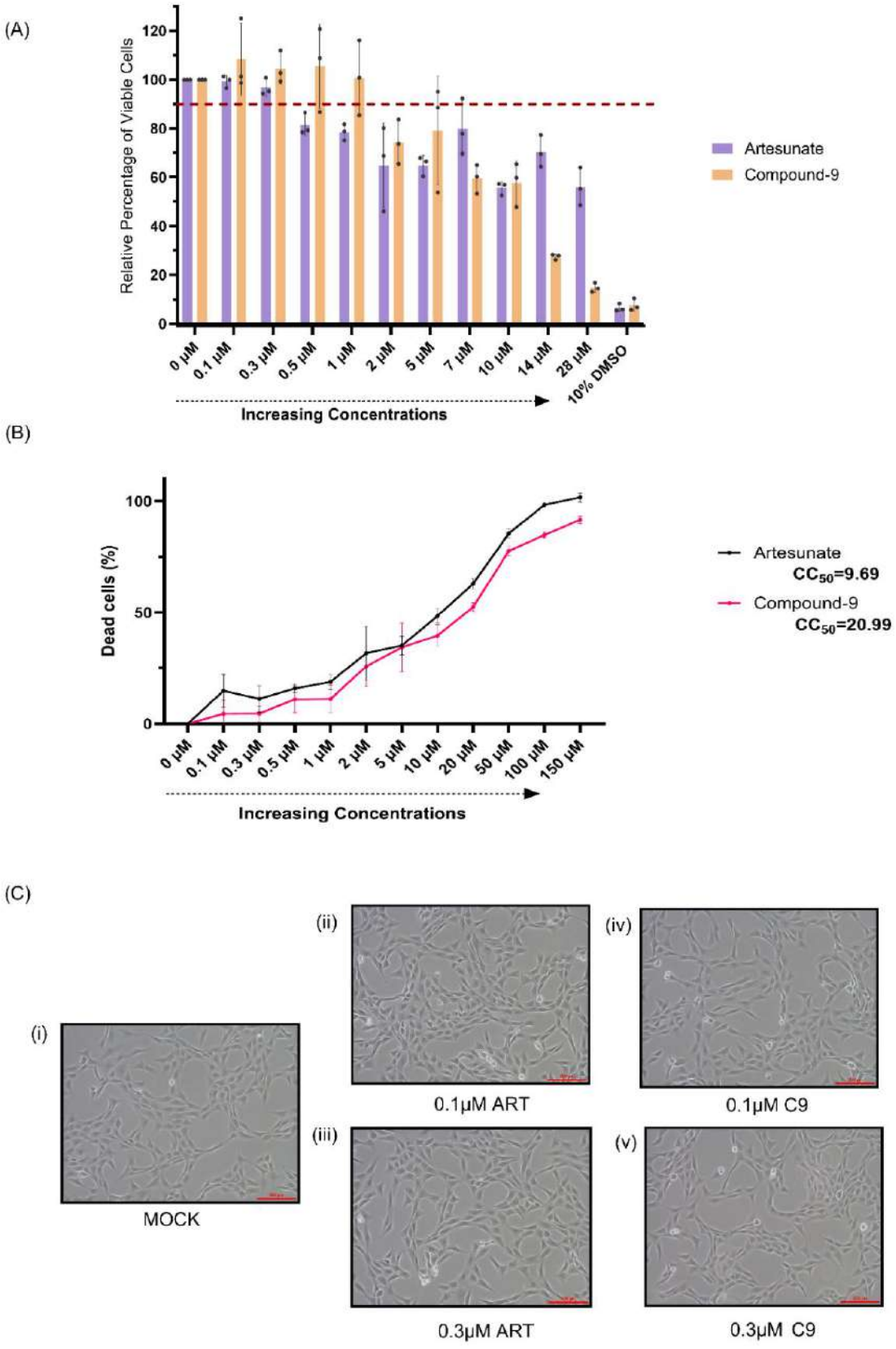

Fig 5.2. Cytotoxic effect of Artesunate and Compound-9 evaluated by performing the cell viability assay and further comparing the morphological changes in HT22 cells post treatment.

(A) Relative percentage of viable cells were measured using the Cell Titer Blue Reagent across increasing concentrations of Artesunate (purple) and Compound-9 (orange). Both compounds showed a dose-dependent decrease in cell viability compared to mock cells (0 µM), with Artesunate exhibiting stronger cytotoxicity at comparable concentrations. (B) Corresponding percentage of dead cells were plotted as a function of drug concentration, indicating CC_{50} values of 9.69 µM for Artesunate and 20.99 µM for Compound-9. Data is represented as mean ± SD of minimum three independent experiments, with individual data points indicated. Statistical analysis was performed using two-way ANOVA followed by Tukey's multiple comparison test. (C) Phase-contrast microscopy images of HT22 cells, C(i)-Mock, C(ii)-0.1µM Art, C(iii)-0.3µM Art, C(iv)-0.1µM C9, C(v)-0.3µM C9 were taken at 20X magnification keeping the scale bar at 200µm showing typical healthy cell morphology across all groups. No signs of cytotoxic damage were observed indicating preserved cell health at these concentrations.

5.3 Art and C9 treatment reduced viral load

5.3.1 Effect of Artesunate and Compound-9 on JEV RNA Expression

To check viral RNA expression in cells treated at different conditions, quantitative real-time PCR was performed. Infection with JEV led to a marked increase in JEV RNA expression compared to the mock control ($p < 0.0001$) for both Artesunate and Compound-9 panels , while GAPDH detection remained consistent across all samples, confirming equal RNA concentration across all samples. Data revealed that treatment with Artesunate at 0.1 µM and 0.3 µM resulted in a modest, dose-dependent reduction in JEV RNA levels compared to JEV-only infected cells; however, these reductions were statistically significant for 0.3µM Art as compared to the 0.1 µM Art dose. Compound-9 treated cells when compared to only-JEV infected cells showed a significant downregulation of the JEV RNA levels at both 0.1 µM ($p = 0.0004$) and 0.3 µM($p=0.0012$) concentrations. No significant changes in JEV RNA levels were observed in the uninfected cells treated with either compound alone (0.1 µM or 0.3 µM), indicating that the observed effects were specific to JEV infection. These results suggested that while both compounds exhibit some antiviral potential, Compound-9 demonstrates a more potent inhibitory effect on JEV replication in HT22 cells compared to Artesunate at the tested concentrations.

5.3.2 Effect of Artesunate and Compound-9 treatment on viral protein load

To assess the impact of Artesunate and Compound-9 on JEV replication, the levels of the viral non-structural protein 3 (NS3) protein expression were evaluated. For this, cell lysate was prepared using protein isolation protocol and subjected to western blot analysis. Densitometric quantification of JEV-NS3 protein was done keeping β-actin as loading control. It revealed significant upregulation of viral protein expression in only JEV infected cells compared to mock controls ($p < 0.0001$). For Artesunate (Fig. 5.3.D), treatment with 0.1 μM showed only a modest reduction in NS3 levels as compared to the and 0.3 μM treatment v/s JEV-infected group ($p = 0.0378$). This suggests that at these concentrations, Artesunate may have a limited effect on inhibiting JEV protein expression. In contrast, Compound-9 treatment (Fig 5.3.E) demonstrated a significant decrease in NS3 expression at both 0.1 μM and 0.3 μM concentrations compared to the JEV-infected group, with p-values of 0.0008 and 0.0059, respectively. These findings indicate that Compound-9 effectively reduces JEV protein expression at non-toxic concentrations in HT22 cells. Representative immunoblots (Fig. 5.3. F,G) confirm the quantitative findings, showing a clear reduction in NS3 band intensity upon treatment with Compound-9.

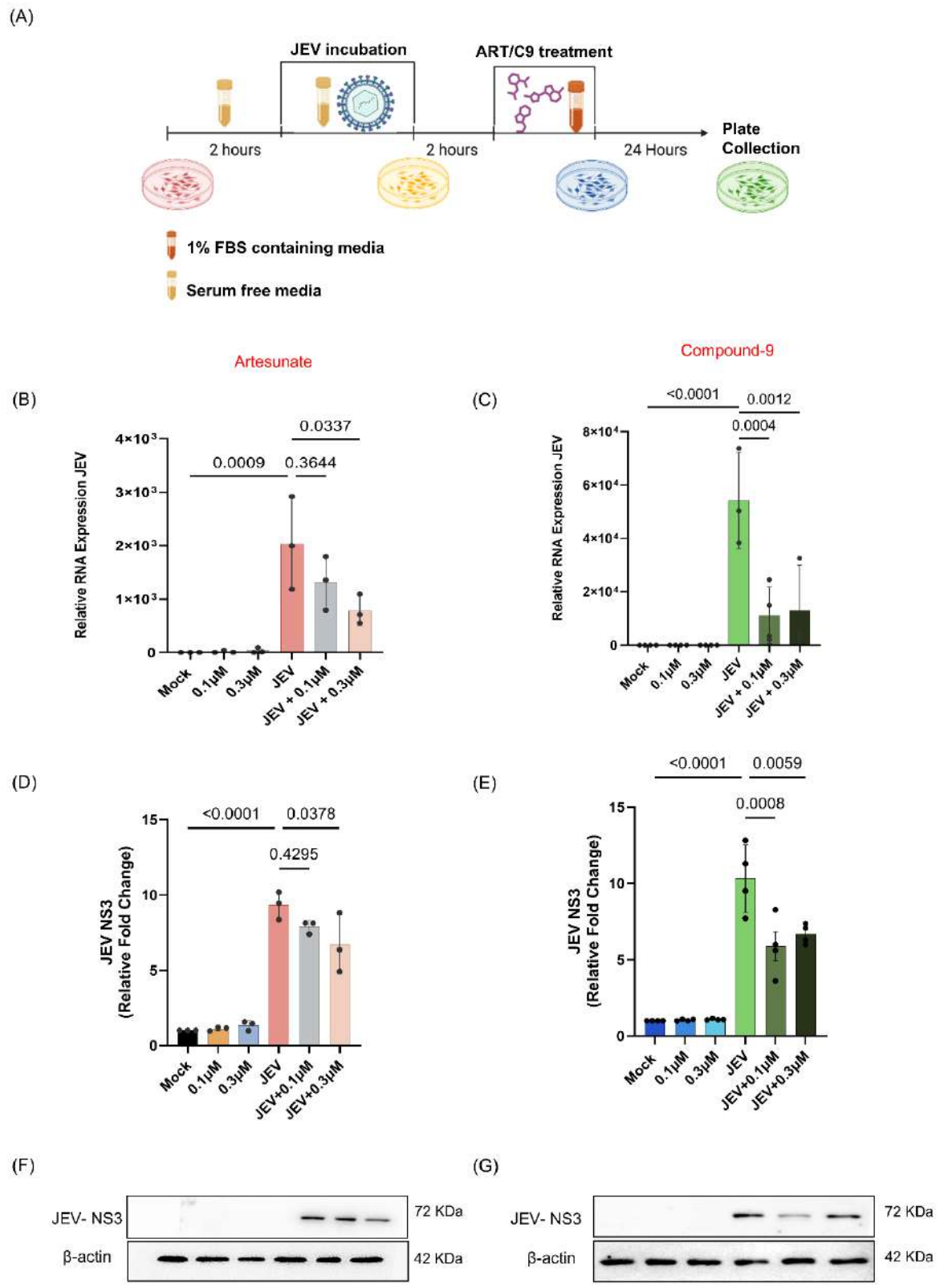

Figure 5.3. **Artesunate and Compound-9 treatment reduced the viral RNA expression and JEV-NS3 protein expression**. As shown in the schematic diagram (A), the treatment paradigm included seeding the HT22 cells and keeping them serum deprived for 2 hours before infecting with JEV at MOI 3. After 2 hours, Art and C9 treatment was added in 1% FBS-DMEM for 24 hours at a concentration of 0.1μM and 0.3μM, following which total RNA was extracted from cells for studying gene expression of viral transcripts using qRT-PCR(B), (C). Fold change was calculated with GAPDH as housekeeping

JEV infection significantly increased viral RNA expression compared to the mock control ($p < 0.0001$), while treatment with Art (0.1μM and 0.3μM) showed a modest reduction in JEV RNA levels but with C9 at same concentrations, a significant reduction in JEV RNA levels was observed ($p = 0.0004$ and $p = 0.0012$, respectively). Analyzing the expression of viral proteins, densitometric quantification of NS3 protein levels (D), (E) was done from western blots (F),(G) keeping β-actin as loading control.NS3 protein expression after Art treatment showed a modest reduction in NS3 levels, treatment with C9 showed a significant reduction at both 0.1 μM and 0.3 μM concentrations compared to JEV, thus supporting the q-PCR analysis. For all experiments, data is represented as mean ± SD of minimum three independent experiments, with individual data points shown. Statistical analysis was performed using ordinary one-way ANOVA followed by Tukey's multiple comparison test.

5.3.3 Immunocytochemistry Analysis of JEV-Infected HT22 Cells

Immunocytochemistry (ICC) staining was done against JEV NS3 protein to visually assess any reduction in the number of infected cells upon treatment with both Artesunate and Compound 9 at 0.1 μM and 0.3 μM concentrations. Although treatment at each dose significantly reduced the percentage of NS3 positive cells ($p < 0.001$) but the graph in fig 5.4 indicated that C-9 at 0.1 μM showed a more pronounced decrease in the number of NS3-positive cells compared to 0.3Mm C9, suggesting better efficacy at the lower dose. Conversely, Artesunate at 0.3 μM demonstrated a more notable reduction in infected cells than at 0.1 μM, confirming the previous dose-dependent trend for this compound. These observations align with the qPCR and Western blot data, further supporting the antiviral potential of both compounds, particularly 0.1 μM Compound-9 and 0.3 μM Artesunate.

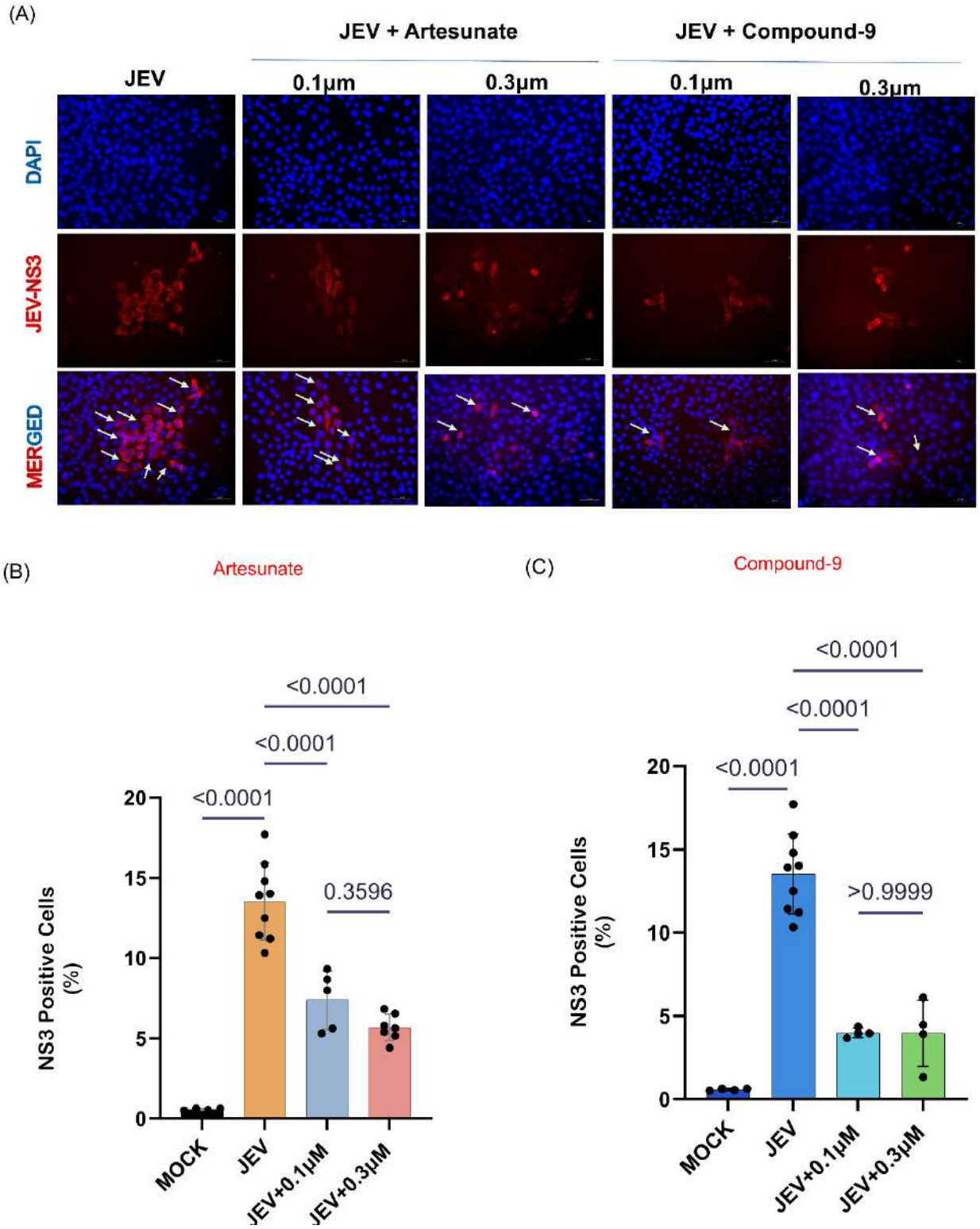

Fig 5.4. Representative ICC images at 40X manignification showing HT22 cells infected with JEV and treated with Artesunate (0.1 µM and 0.3 µM) or Compound-9 (0.1 µM and 0.3 µM). In treated groups, a significant reduction was observed in the no. of NS3-positive cells (red) compared to untreated JEV-infected controls.

5.4 Inspecting oxidative stress and inflammation in HT22 cells post Art and C9 treatment

Oxidative and nitrosative stress are two key hallmarks of JEV infection in the neuronal cells, contributing to cellular damage and inflammation. In this study, we evaluated the levels of reactive oxygen species (ROS) and nitric oxide (NO) in HT22 cells infected with JEV and treated with either artesunate or compound-9 at two concentrations (0.1 μM and 0.3 μM). ROS levels were measured using DCFDA-based fluorescence assays, while NO levels were quantified using the Griess reagent. Further inflammatory response was measured post treatment by analyzing the p-NFκB levels.

5.4.1 Art and C9 treatment inhibit neuronal death by reducing ROS production

As reactive oxygen species (ROS) are major microbicidal molecules, ROS levels were found to be significantly higher in JEV infected cells compared to mock-infected cells thus confirming the role of oxidative stress during JEV infection. Treatment with artesunate reduced ROS levels in JEV-infected cells. Both 0.1 μM and 0.3 μM doses led to a decrease, with 0.3 μM showing a slightly stronger reduction. However, ROS levels in treated cells remained significantly higher than in mock controls, suggesting that while artesunate has antioxidant properties, it does not fully normalize ROS levels at the tested concentrations. Compound-9 treatment also led to a decrease in ROS levels. Interestingly, the 0.1 μM dose was more effective in reducing ROS compared to 0.3 μM, indicating a potential concentration-dependent paradoxical effect where lower doses of compound-9 exert stronger antioxidant activity.

5.4.2 Effects of Artesunate and Compound-9 on JEV-Induced NO Levels

JEV infection significantly elevated NO production by approximately 1.3-fold compared to the mock group, indicating enhanced nitrosative stress upon viral infection.Treatment with either artesunate or compound-9 effectively reduced NO levels in infected cells. At the 0.1 μM concentration, both compounds decreased NO production to about 1.05–1.1-fold, while the 0.3

μM concentration resulted in slightly higher NO levels, around 1.1–1.15-fold. Notably, the lower dose of compound-9 (0.1 μM) showed a more pronounced suppressive effect on NO compared to its higher dose, whereas artesunate demonstrated a dose-dependent reduction. However, at 0.3 μM, artesunate appeared more effective than compound-9 in restoring NO levels closer to baseline.

5.4.3 Effects of Artesunate and Compound-9 on JEV-Induced inflammation

To investigate the inflammatory response during JEV infection, western blot analysis was performed to measure the levels of phosphorylated NF-κB (p-NFκB) as it is a key regulator of pro-inflammatory gene expression in viral infections. Figure 5.5. (E-H) indicates the significantly elevated p-NFκB/NFκB ratio in JEV infected cells as compared to their mock groups, thus confirming the activation of NF-κB pathway. Post-infection treatment with artesunate at 0.3 μM significantly reduced this activation ($p = 0.0169$ vs. JEV), while the 0.1 μM dose showed a trend toward reduction ($p = 0.0694$), though not statistically significant. Post-treatment with compound 9 at both 0.1 μM and 0.3 μM led to a significant decrease in p-NFκB levels ($p = 0.0099$ and 0.0140 vs. JEV, respectively), restoring them nearly to baseline levels ($p = 0.9967$ vs. mock). For densitometric quantification, blots for p-NFκB were normalized to total NFκB and β-actin to account for loading variability.

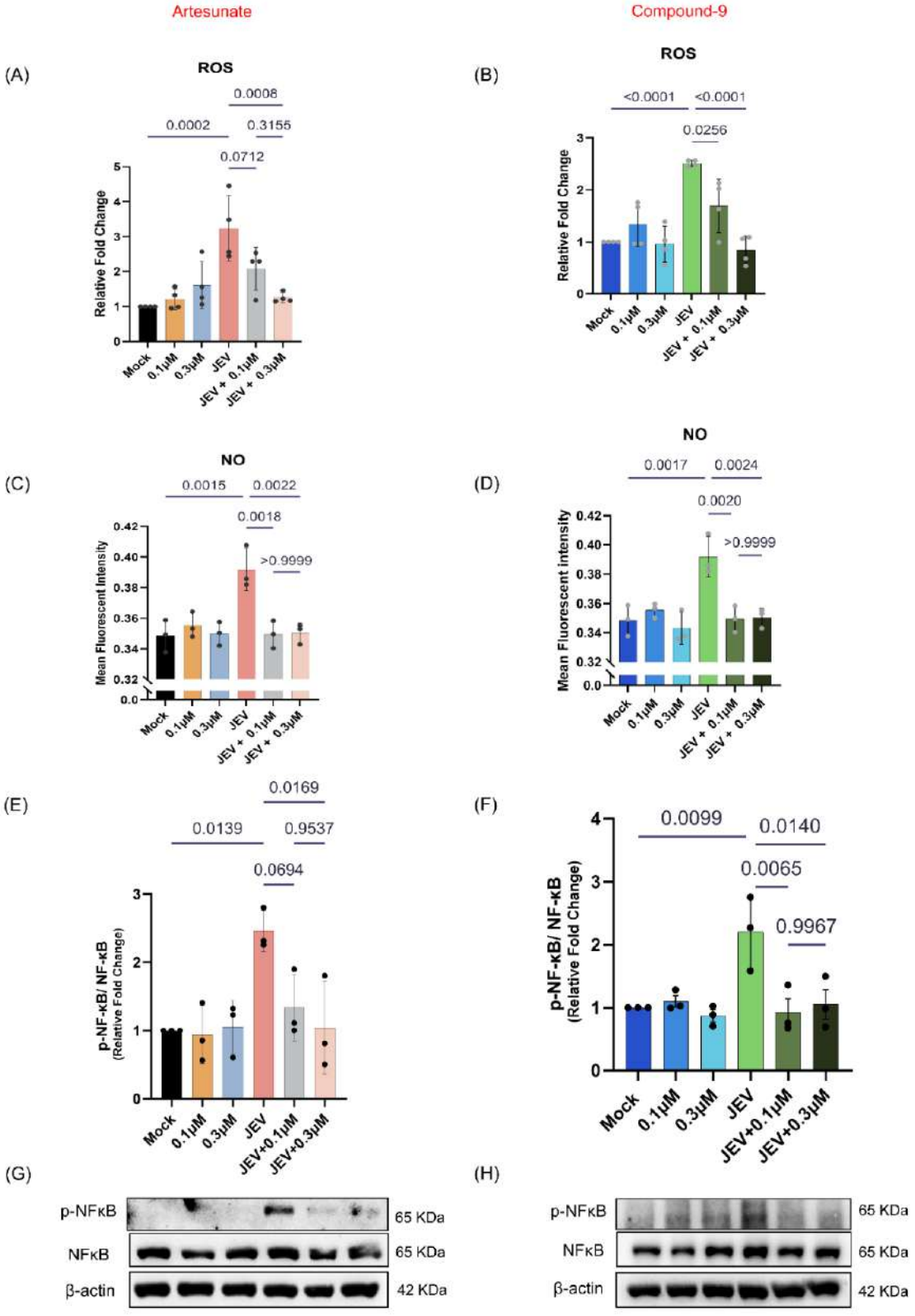

Fig 5.5. Artesunate and Compound-9 reduce JEV-induced oxidative stress and inflammation in HT22 cells. Bar graphs show the fold change in levels of ROS (A, B), NO (C, D) and p-NFκB (E, F). JEV infection significantly elevated ROS, NO and p-NFκB production, which was attenuated by both drug treatments. Data represent mean ± SD (n = 3). Statistical significance was determined using one-way ANOVA with Tukey's post hoc test.

5.5 Artesunate and Compound-9 reduced virus-induced apoptotic cell death

Annexin V/PI staining revealed a marked increase in the percentage of apoptotic HT22 cells following JEV infection, confirming virus-induced cytotoxicity. In comparison to the mock group, JEV-infected cells showed a significant increase in apoptosis ($p < 0.0001$). Treatment with both artesunate and compound-9 reduced the percentage of apoptotic cells, indicating a protective effect. Artesunate significantly lowered apoptosis at both 0.1 μM and 0.3 μM concentrations compared to the JEV group ($p = 0.0006$ and $p = 0.0002$, respectively), with a slightly stronger effect observed at 0.3 μM. Similarly, compound-9 significantly attenuated JEV-induced apoptosis at both doses, with a more pronounced effect ($p < 0.0001$) at both at 0.1 μM and 0.3 μM dose. These findings suggest that both compounds can mitigate JEV-induced apoptosis, though their optimal protective doses may vary.

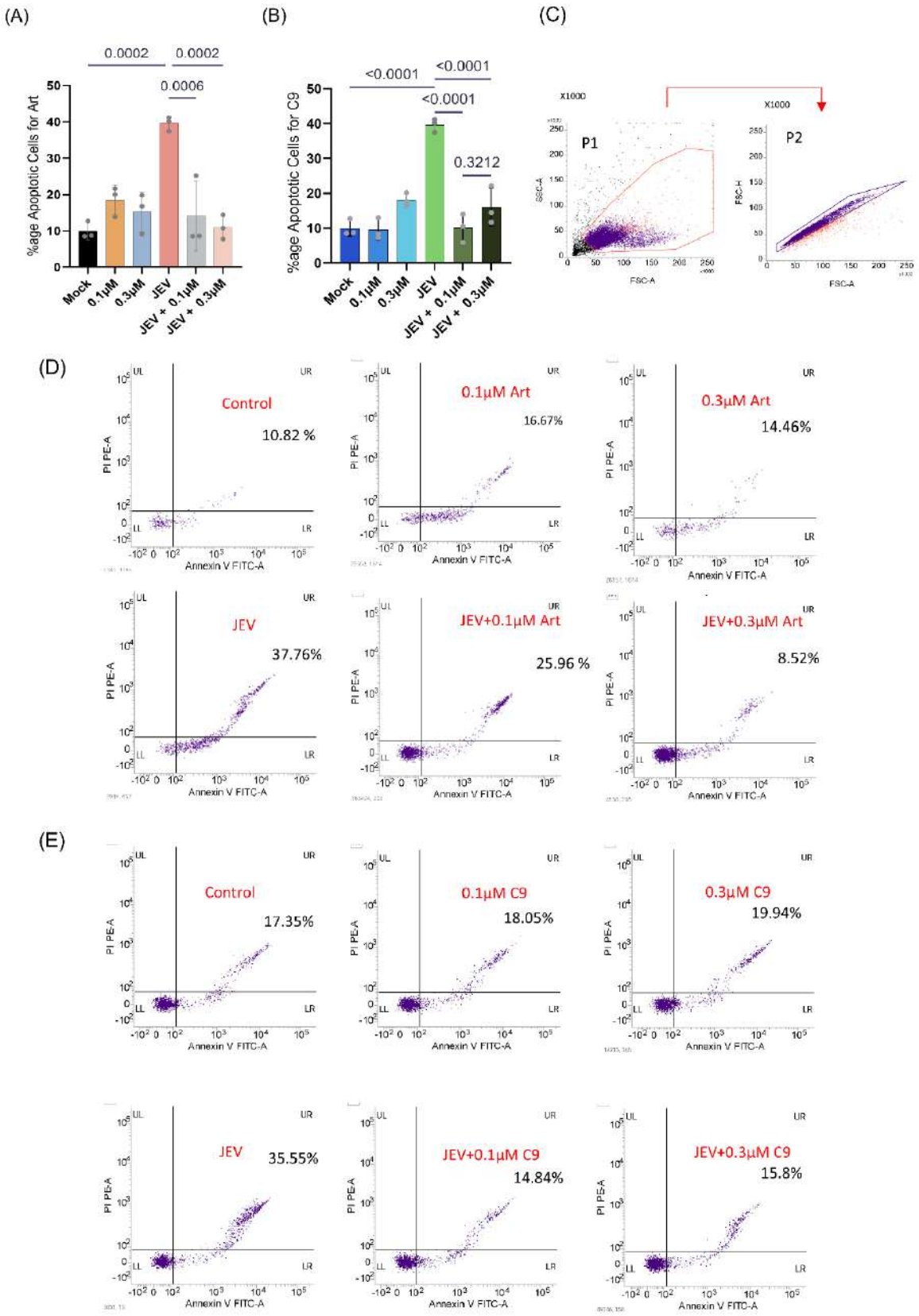

Fig 5.6. **Annexin V/PI staining indicating attenuated JEV-induced apoptosis** in HT22 cells by Artesunate (D) and Compound-9 (E) treatment. Bar graphs (A), (B) depict the percentage of apoptotic cells measured 24 h post-infection. (C) Represents the selected parent population of cells. Data represent mean ± SD (n = 3). Statistical significance was calculated using one-way ANOVA with Tukey's multiple comparisons test.

5.6 Evaluating the efficacy of Art and C9 *In vivo*

5.6.1 Establishing JEV infection in BALB/c mice

To establish JEV infection, JEV strain JaOArS982 was intraperitoneally injected into the BALB/c post-natal day 10 mice and they were kept under observation for next few upcoming days. Post infection, the overall mice health and body weight was recorded each day and we found a drastic weight loss in JEV infected animals from 5th day onwards. The weight continued to decrease till the animals were terminally ill on 6 days post infection (6dpi) (Fig-7b) with symptoms including piloerection, hunchback, restricted movement, tip toeing, and seizures in some of the severely ill cases. None of the infected animals survived 8 dpi indicating a median survival rate of only 6dpi with manifestation of full symptoms. The full symptom terminally ill mice brain was then collected.

5.6.2 Art and C9 enhanced the survival outcomes in JEV-infected BALB/c mice

Kaplan–Meier survival analysis was performed on JEV-infected BALB/c mice treated with varying doses (3, 7, and 10 mg/kg) of the two compounds. As expected, the JEV-infected untreated group (N=13) showed a sharp decline in survival, with no animals surviving beyond 8 days post-infection.

At the 3 mg/kg dose, both Artesunate and Compound-9 improved survival significantly compared to the untreated JEV group. However, compound-9-treated mice exhibited marginally higher survival rates (N=13; p=0.0027) than the Artesunate group (N=11; p=0.0194), suggesting a dose-responsive therapeutic effect of both compounds, with C9 showing better potency.

At the 7 mg/kg dose, survival was markedly improved in both treatment groups. While Artesunate and Compound-9 each resulted in ~62.5% SURVIVAL (N=8 for both groups; p<0.0001 Vs JEV), the onset of death was delayed in the C9 group, indicating better disease mitigation in early post-infection days.

At the 10 mg/kg dose, both Artesunate and Compound-9 provided robust protection (p<0.0001 vs JEV), with the compound-9-treated mice maintaining a longer plateau phase in survival. Although the overall survival percentage was similar between the two, the C9 group displayed slightly improved early-phase protection, hinting at superior pharmacodynamic properties. Statistical analysis for this curve was performed using the log-rank (Mantel-Cox) test, and p-values confirmed the increased survival probabilities by both treatments.

5.6.3 Art and C9 preserved the physiological weight gain in JEV-infected mice

Body weight was monitored daily for 30 days as an indicator of overall survival health and disease progression in JEV-infected BALB/c mice treated with Artesunate and Compound-9 at varying doses. As compared to the observable weight loss in untreated JEV-infected mice on 7 dpi, which was consistent with severe infection and high mortality, treatment with either Artesunate or Compound-9 helped to attenuate this weight loss.

As shown in Fig 5.7.(C), Treatment with artesunate (3 mg/kg) and compound-9 (3 mg/kg) individually led to partial mitigation of weight loss, with animals showing modest recovery after 10 dpi. However, higher doses of 7 mg/kg for both the compounds were associated with improved weight recovery, particularly after 12 dpi. Notably, the 10 mg/kg treatment groups exhibited near-complete recovery in body weight trajectory, closely resembling the mock control. Among all groups, the JEV + compound-9 (10 mg/kg) group demonstrated the highest mean body weight by 30 dpi, indicating superior efficacy. Overall, these results suggest a dose-dependent protective effect of both artesunate and compound-9 in JEV infection as higher doses showed enhanced efficacy in preserving normal growth patterns.

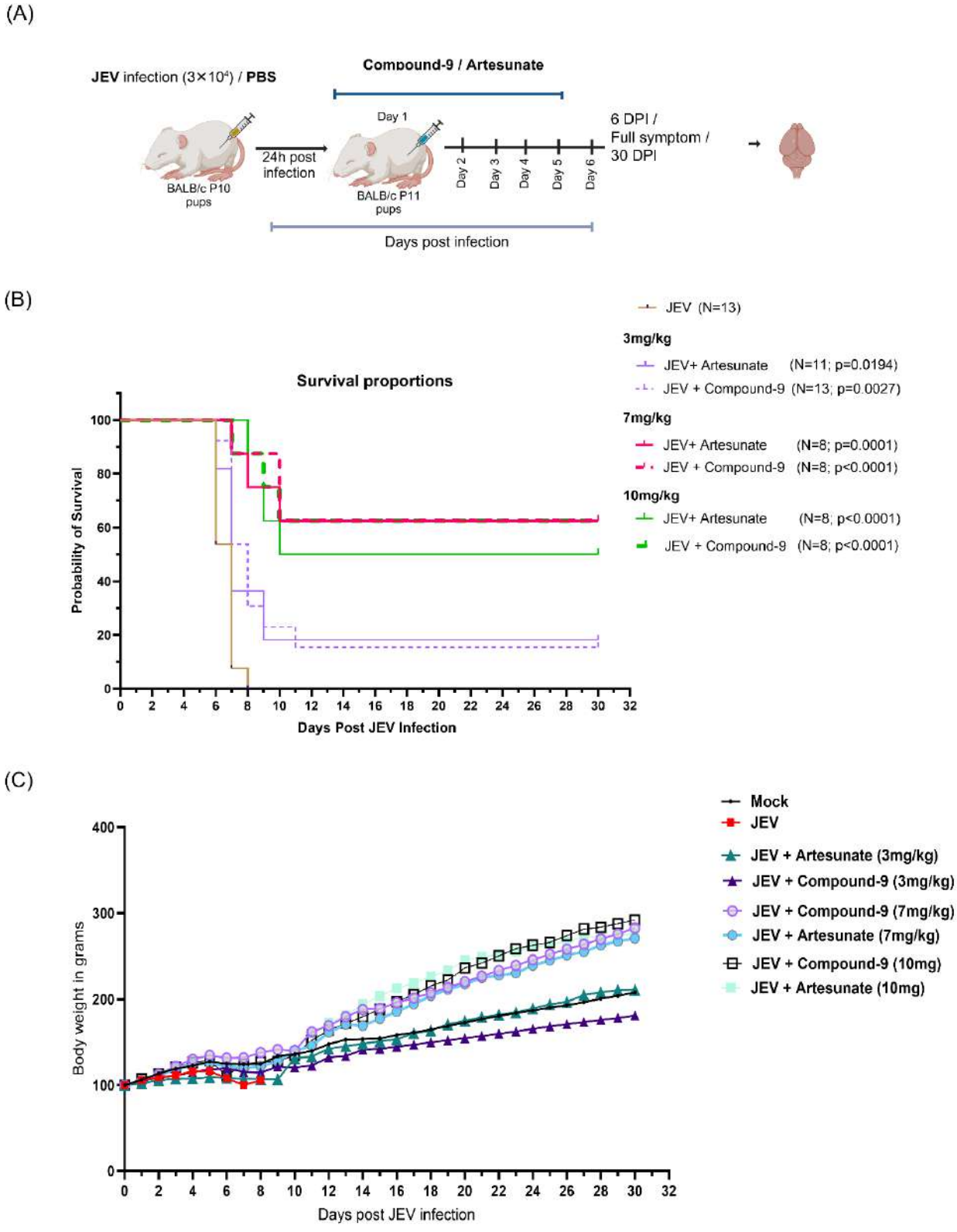

Fig 5.7. In-vivo efficacy of Art and C9 Treatment against JEV.
Art and C9 treatment significantly increased survival chances in JEV infected BALB/c mice when treated as represented in the experimental scheme (A). Plots depicting the Kaplan-Meir curve indicating the survival probabilities (B) and the body weights (C) of JEV infected mice treated with either of the compounds at 3mg/kg, 7mg/kg or 10mg/kg. Statistical significance was determined using Log-rank (Mantel-Cox) test and graphs were plotted with a minimum of n=8 mice

Chapter 6

DISCUSSION

This study explored the antiviral and neuroprotective potential of Artesunate and its novel derivative, Compound-9 (C9) against Japanese Encephalitis Virus (JEV) infection in HT22 neuronal cells. As Japanese Encephalitis Virus (JEV) is a neurotropic flavivirus, it predominantly infects neurons through direct viral replication, inflammatory cascades, oxidative stress, and apoptosis[67]. In this context, the present study explored the antiviral efficacy of Artesunate (Art), a clinically approved antimalarial drug which has previously shown promise for repurposing due to its anti-inflammatory[68] and antiviral properties[54]. With no targeted antiviral therapy currently available, drug repurposing offers a viable strategy for rapid therapeutic intervention. According to the previous literature, naphthalimides and its derivatives, especially naphthalene diimides (NDIs) have reported the ability to bind DNA and RNA structures especially G-quadruplexes, which are rich in guanine and found in cancer and viral genomes (e.g., HIV-1), hence imparting significant antitumor and antiviral therapeutic potential[65,66]. With the aim of enhancing bioactivity and cellular efficacy of Artesunate, it was conjugated with a napthalamide moiety to synthesize compound-9 and it's structural composition was confirmed by NMR at Dr. Hossain's laboratory. A series of molecular and cellular assays were performed to systematically assess the comparative antiviral therapeutic efficacy of these compounds, and lay the groundwork for further mechanistic and preclinical evaluations.

To begin with, cell viability assay was performed to determine the therapeutic range and differential cytotoxic effects of Art and C9. Both compounds exhibited a concentration-dependent decrease in cell viability, with higher concentrations leading to greater cytotoxicity. These findings aligned well with the known pharmacological profile of Art, which exhibited potent cytotoxic activity in various cell lines[54,69] whereas Compound-9 demonstrated a more gradual increase in cytotoxicity, potentially offering a broader therapeutic range. To further validate the cytotoxicity data, lower concentrations of 0.1 μM and 0.3 μM were selected for

both Artesunate and Compound-9 as they showed a preferable high percentage of viable cells at these concentrations. At these low concentrations, phase-contrast microscopy images were taken which revealed healthy neuronal characteristics of treated cells same as in mock cells suggesting both the compounds were tolerated well by HT22 cells at these doses.

Quantitative Real time PCR confirmed a successful infection and robust viral replication as JEV infection led to a substantial increase in viral gene expression compared to mock-infected controls. Treatment with both Art and C9 resulted in a dose-dependent reduction in viral RNA levels; however, C9 exhibited a more pronounced suppression, particularly at 0.1 µM, where the decrease was statistically significant. This trend was further validated at the protein level via densitometric quantification of JEV NS3 immunoblots. NS3 is a key non-structural protein essential for viral replication. Images from Immunocytochemistry (ICC) further substantiated these findings by showing visibly fewer infected cells in drug-treated groups. C9 at 0.1 µM resulted in the lowest number of NS3-positive cells reinforcing the notion that C9, even at a lower concentration, is more effective in curbing infection.

Given that viral infections often elevate oxidative stress, we next assessed intracellular reactive oxygen species (ROS) and nitric oxide (NO) levels. JEV infection markedly increased ROS and NO which are well-documented contributors to neuronal damage and neuroinflammation in viral encephalitis[67]. Both Art and C9 treatments significantly curtailed these increased oxidative stress markers. Notably, C9 led to a greater fold reduction in ROS and NO than Art, particularly at the 0.1 µM concentration. This suggested superior antioxidative properties of C9, possibly contributing to better preservation of neuronal integrity during infection. These stress responses

To evaluate drug-induced modulation of apoptosis, Annexin V-PI flow cytometry was performed. JEV infection triggered a substantial rise in apoptotic cells. Both compounds significantly reversed this effect, with 0.1 µM C9 dose bringing apoptosis levels close to

baseline, while Art had a milder effect, especially at the lower concentration. This anti-apoptotic effect may be a consequence of reduced viral replication and diminished oxidative stress, aligning with the multifaceted protective action of C9.

Based on these promising *in vitro* findings, an *in vivo* paradigm was designed to evaluate the efficacy of Compound-9 in JEV infected Balb/c mice and further validate its therapeutic potential in a more physiologically relevant system. Previous reports of survival analysis[70] revealed that while JEV infected mice had a median survival of 6 days and showed severe JE symptoms such as hunchback, pilorection and restricted movement along with a significant weight loss from 4dpi, both the drugs conferred statistically significant protection in a dose-dependent manner. However, Compound-9-treated mice at all doses, particularly 7 mg/kg and 10 mg/kg, exhibited better survival rates and delayed mortality compared to Artesunate, suggesting enhanced antiviral potency and systemic protection. In parallel, monitoring of body weight trends served as a physiological marker of health. While JEV-infected mice experienced marked weight loss, treatment with Compound-9 led to a more robust and earlier recovery of body weight, aligning with improved survival outcomes. Artesunate-treated mice displayed slower recovery, indicating relatively limited physiological protection.Taken together, these results suggest that Compound-9 confers greater survival benefits *in vivo* over its parent compound, artesunate, offering both improved survival and better maintenance of overall health during JEV infection.

Chapter 7

CONCLUSION

This study highlights the evidence for the enhanced anti-JEV efficacy of Compound-9, a novel derivative of Artesunate. C9 not only suppressed viral replication more effectively but also consistently outperformed its parent compound.by alleviating the collateral oxidative and apoptotic damage typically associated with neurotropic viral infections. Supporting this, immunocytochemical staining showed fewer NS3-positive cells in C9 conditions, with 0.1 µM being notably more effective than 0.3 µM—highlighting its potent activity even at lower concentrations.*In vivo* studies corroborated these findings. Kaplan–Meier survival curves indicated a significant improvement in survival of BALB/c mice treated with C9 at 3, 7, and 10 mg/kg, with superior outcomes compared to Art at the same doses. These findings support Compound-9 as a promising next-generation candidate for JEV therapeutics, with advantages in both antiviral efficacy and neuroprotection.

APPENDICES

1. Components of electrode buffer (1L)

Components	Amount
Tris Base	3.03g
Glycine	14.4g
SDS	1g
DW	1L

2. Components of Transfer Buffer (1L)

Components	Amount
Tris Base	3.03g
Glycine	14.4g
Methanol	200mL
DW	800mL

3. Components of Ponceau (100mL)

Components	Amount
Ponceau	100mg
MQ	95mL
GAA	5mL

4. 1.5 M Tris-HCl pH-8.8 (200ml)

Components	Amount
Tris	36.3g
MQ	95mL
	pH adjusted using HCl

5. 0.5 M Tris-HCl pH-6.8 (200ml)

Components	Amount
Tris	12.1g
MQ	95mL
	pH adjusted using HCl

6. 10% Resolving Gel

Components	Volume (mL)
Sterile Distilled Water	4000
Acrylamide (30%)	3300
Tris (1.0M) pH 6.8	2500
SDS (10%)	100
APS (10%)	100
TEMED	10

7. 4% Resolving Gel

Components	Volume (mL)
Sterile Distilled Water	3050
Acrylamide (30%)	667
Tris (1.0M) pH 6.8	1.25
SDS (10%)	50
APS (10%)	50
TEMED	10

LIST OF TABLES

Table 1. Antibody dilutions

Antibody	Cat#	Raised in	Dilutions	Mol. Wt. (kDa)
JEV NS3	GTX125868	Rb	1:75000	73
p-NFκβ	CST-3031L	Rabbit	1:2000	65
t- NFκβ	8242S	Rabbit	1:2000	65
β-actin	A3854	Rabbit	1:100000	42

Table 2. Primer Sequences used in RT-PCR

Gene Name	Primer sequence
JaOAr	Forward: 5' AGAGCGGGGAAAAAGGTCAT 3' Reverse: 5' TTTCACGCTCTTTCTACAGT 3'
GAPDH	Forward: 5' ATGGGGGAAGGTGAAGGTCG 3' Reverse: 5' GGGGTCATTGATGGCAACAATA 3'

Table 3. Components of incomplete lysis buffer (10ml)

COMPONENTS	VOLUME (µL)
Triton X 100	100
NaCl	300
Tris-HCl pH 7.4	100
0.5 M EDTA	20
0.1 M EGTA	100
NP40/ IGEPAL	50
MQ	Make up volume to 50 ml

REFERENCES

1. Louten J. Chapter 2 - Virus Structure and Classification. In: Louten J, ed. *Essential Human Virology*. Academic Press; 2016:19-29. doi:10.1016/B978-0-12-800947-5.00002-8

2. Neurotropic virus infections as the cause of immediate and delayed neuropathology | Acta Neuropathologica. Accessed May 16, 2025. https://link.springer.com/article/10.1007/s00401-015-1511-3

3. Abdullahi AM, Sarmast ST, Singh R. Molecular Biology and Epidemiology of Neurotropic Viruses. *Cureus*. 2020;12(8):e9674. doi:10.7759/cureus.9674

4. Kibenge FSB. Chapter 2 - Classification and Identification of Aquatic Animal Viruses. In: Kibenge FSB, Godoy MG, eds. *Aquaculture Virology*. Academic Press; 2016:9-34. doi:10.1016/B978-0-12-801573-5.00002-4

5. Boruah AP, Thakur KT. Arthropod-borne encephalitis: an overview for the clinician and emerging considerations. *Postgrad Med J*. 2023;99(1174):826-833. doi:10.1136/pmj-2022-142002

6. Srichawla BS, Manan MR, Kipkorir V, et al. Neuroinvasion of emerging and re-emerging arboviruses: A scoping review. *SAGE Open Med*. 2024;12:20503121241229847. doi:10.1177/20503121241229847

7. Ugolini G. Chapter 10 - Rabies Virus as a Transneuronal Tracer of Neuronal Connections. In: Jackson AC, ed. *Advances in Virus Research*. Vol 79. Research Advances in Rabies. Academic Press; 2011:165-202. doi:10.1016/B978-0-12-387040-7.00010-X

8. Smith G. Herpesvirus Transport to the Nervous System and Back Again. *Annu Rev Microbiol*. 2012;66(Volume 66, 2012):153-176. doi:10.1146/annurev-micro-092611-150051

9. Mori I, Nishiyama Y, Yokochi T, Kimura Y. Olfactory transmission of neurotropic viruses. *J Neurovirol*. 2005;11(2):129-137. doi:10.1080/13550280590922793

10. Koyuncu OO, Hogue IB, Enquist LW. Virus Infections in the Nervous System. *Cell Host Microbe*. 2013;13(4):379-393. doi:10.1016/j.chom.2013.03.010

11. Yun SI, Lee YM. Early Events in Japanese Encephalitis Virus Infection: Viral Entry. *Pathogens*. 2018;7(3):68. doi:10.3390/pathogens7030068

12. Mukherjee S, Sengupta N, Chaudhuri A, et al. PLVAP and GKN3 Are Two Critical Host Cell Receptors Which Facilitate Japanese Encephalitis Virus Entry Into Neurons. *Sci Rep*. 2018;8(1):11784. doi:10.1038/s41598-018-30054-z

13. Beyond the Surface: Endocytosis of Mosquito-Borne Flaviviruses. Accessed May 16, 2025. https://www.mdpi.com/1999-4915/13/1/13

14. Chu JJH, Ng ML. Infectious Entry of West Nile Virus Occurs through a Clathrin-Mediated Endocytic Pathway. *J Virol*. 2004;78(19):10543-10555. doi:10.1128/JVI.78.19.10543-10555.2004

15. Barrows NJ, Campos RK, Liao KC, et al. Biochemistry and Molecular Biology of Flaviviruses. *Chem Rev*. 2018;118(8):4448-4482. doi:10.1021/acs.chemrev.7b00719

16. Anwar MN, Akhtar R, Abid M, et al. The interactions of flaviviruses with cellular receptors: Implications for virus entry. *Virology*. 2022;568:77-85. doi:10.1016/j.virol.2022.02.001

17. Miller S, Krijnse-Locker J. Modification of intracellular membrane structures for virus replication. *Nat Rev Microbiol*. 2008;6(5):363-374. doi:10.1038/nrmicro1890

18. Sharma KB, Vrati S, Kalia M. Pathobiology of Japanese encephalitis virus infection. *Mol Aspects Med*. 2021;81:100994. doi:10.1016/j.mam.2021.100994

19. Solomon T, Dung NM, Kneen R, Gainsborough M, Vaughn D, Khanh VT. Japanese encephalitis. *J Neurol Neurosurg Psychiatry*. 2000;68(4):405-415. doi:10.1136/jnnp.68.4.405

20. Pfeffer M, Dobler G. Emergence of zoonotic arboviruses by animal trade and migration. *Parasit Vectors*. 2010;3:35. doi:10.1186/1756-3305-3-35

21. Vector-free transmission and persistence of Japanese encephalitis virus in pigs | Nature Communications. Accessed May 16, 2025. https://www.nature.com/articles/ncomms10832

22. García-Nicolás O, Braun RO, Milona P, et al. Targeting of the Nasal Mucosa by Japanese Encephalitis Virus for Non-Vector-Borne Transmission. *J Virol*. 2018;92(24):e01091-18. doi:10.1128/JVI.01091-18

23. Turtle L, Solomon T. Japanese encephalitis - the prospects for new treatments. *Nat Rev Neurol*. 2018;14(5):298-313.

24. Pearce JC, Learoyd TP, Langendorf BJ, Logan JG. Japanese encephalitis: the vectors, ecology and potential for expansion. *J Travel Med*. 2018;25(suppl_1):S16-S26. doi:10.1093/jtm/tay009

25. Mulvey P, Duong V, Boyer S, et al. The Ecology and Evolution of Japanese Encephalitis Virus. *Pathogens*. 2021;10(12):1534. doi:10.3390/pathogens10121534

26. Japanese encephalitis in north Queensland, Australia, 1998 - Hanna - 1999 - Medical Journal of Australia - Wiley Online Library. Accessed May 16, 2025. https://onlinelibrary.wiley.com/doi/abs/10.5694/j.1326-5377.1999.tb127878.x?msockid=1b473c712951695805412f83286968f5

27. Gao X, Liu H, Li X, et al. Changing Geographic Distribution of Japanese Encephalitis Virus Genotypes, 1935-2017. *Vector Borne Zoonotic Dis Larchmt N*. 2019;19(1):35-44. doi:10.1089/vbz.2018.2291

28. Yang DK, Oh YI, Kim HR, et al. Serosurveillance for Japanese encephalitis virus in wild birds captured in Korea. *J Vet Sci*. 2011;12(4):373-377. doi:10.4142/jvs.2011.12.4.373

29. Antibodies to Flaviviruses in Wild Ducks Captured in Hokkaido, Japan: Risk Assessment of Invasive Flaviviruses. ResearchGate. Accessed May 16, 2025. https://www.researchgate.net/publication/26281059_Antibodies_to_Flaviviruses_in_Wild_Ducks_Captured_in_Hokkaido_Japan_Risk_Assessment_of_Invasive_Flaviviruses

30. Huang YJS, Harbin JN, Hettenbach SM, et al. Susceptibility of a North American Culex quinquefasciatus to Japanese Encephalitis Virus. *Vector-Borne Zoonotic Dis*. 2015;15(11):709-711. doi:10.1089/vbz.2015.1821

31. Yadav P, Chakraborty P, Jha NK, et al. Molecular Mechanism and Role of Japanese Encephalitis Virus Infection in Central Nervous System-Mediated Diseases. *Viruses*. 2022;14(12):2686. doi:10.3390/v14122686

32. A structural perspective of the flavivirus life cycle. CoLab. Accessed May 17, 2025. https://colab.ws/articles/10.1038%2Fnrmicro1067

33. Unni SK, Růžek D, Chhatbar C, Mishra R, Johri MK, Singh SK. Japanese encephalitis virus: from genome to infectome. *Microbes Infect*. 2011;13(4):312-321. doi:10.1016/j.micinf.2011.01.002

34. Ding D, Kilgore PE, Clemens JD, Wei L, Zhi-Yi X. Cost-effectiveness of routine immunization to control Japanese encephalitis in Shanghai, China. *Bull World Health Organ*. 2003;81(5):334-342.

35. Liao CL, Lin YL, Shen SC, et al. Antiapoptotic but Not Antiviral Function of Human bcl-2 Assists Establishment of Japanese Encephalitis Virus Persistence in Cultured Cells. *J Virol*. 1998;72(12):9844. doi:10.1128/jvi.72.12.9844-9854.1998

36. Leung JY, Pijlman GP, Kondratieva N, Hyde J, Mackenzie JM, Khromykh AA. Role of Nonstructural Protein NS2A in Flavivirus Assembly. *J Virol*. 2008;82(10):4731-4741. doi:10.1128/jvi.00002-08

37. Wahaab A, Liu K, Hameed M, et al. Identification of Cleavage Sites Proteolytically Processed by NS2B-NS3 Protease in Polyprotein of Japanese Encephalitis Virus. *Pathogens*. 2021;10(2):102. doi:10.3390/pathogens10020102

38. Fang J, Li H, Kong D, et al. Structure-based discovery of two antiviral inhibitors targeting the NS3 helicase of Japanese encephalitis virus. *Sci Rep*. 2016;6(1):34550. doi:10.1038/srep34550

39. Luo D, Vasudevan SG, Lescar J. The flavivirus NS2B-NS3 protease-helicase as a target for antiviral drug development. *Antiviral Res*. 2015;118:148-158. doi:10.1016/j.antiviral.2015.03.014

40. Utama A, Shimizu H, Morikawa S, et al. Identification and characterization of the RNA helicase activity of Japanese encephalitis virus NS3 protein. *FEBS Lett*. 2000;465(1):74-78. doi:10.1016/S0014-5793(99)01705-6

41. Matusan AE, Pryor MJ, Davidson AD, Wright PJ. Mutagenesis of the Dengue Virus Type 2 NS3 Protein within and outside Helicase Motifs: Effects on Enzyme Activity and Virus Replication. *J Virol*. 2001;75(20):9633-9643. doi:10.1128/JVI.75.20.9633-9643.2001

42. Fang J, Li H, Kong D, et al. Structure-based discovery of two antiviral inhibitors targeting the NS3 helicase of Japanese encephalitis virus. *Sci Rep*. 2016;6(1):34550. doi:10.1038/srep34550

43. Agarwal A, Alam MohdF, Basu B, et al. Japanese Encephalitis Virus NS4A Protein Interacts with PTEN-Induced Kinase 1 (PINK1) and Promotes Mitophagy in Infected Cells. *Microbiol Spectr*. 10(3):e00830-22. doi:10.1128/spectrum.00830-22

44. Kaufusi PH, Tseng AC, Kelley JF, Nerurkar VR. Selective Reactivity of Anti-Japanese Encephalitis Virus NS4B Antibody Towards Different Flaviviruses. *Viruses*. 2020;12(2):212. doi:10.3390/v12020212

45. Yun SI, Lee YM. Japanese encephalitis. *Hum Vaccines Immunother*. 2014;10(2):263-279. doi:10.4161/hv.26902

46. Banerjee A, Tripathi A. Recent advances in understanding Japanese encephalitis. *F1000Research*. 2019;8:F1000 Faculty Rev-1915. doi:10.12688/f1000research.19693.1

47. Patabendige A, Michael BD, Craig AG, Solomon T. Brain microvascular endothelial-astrocyte cell responses following Japanese encephalitis virus infection in an *in vitro* human blood-brain barrier model. *Mol Cell Neurosci*. 2018;89:60-70. doi:10.1016/j.mcn.2018.04.002

48. German AC, Myint KSA, Mai NTH, et al. A preliminary neuropathological study of Japanese encephalitis in humans and a mouse model. *Trans R Soc Trop Med Hyg*. 2006;100(12):1135-1145. doi:10.1016/j.trstmh.2006.02.008

49. Regulation of inflammation in Japanese encephalitis | Journal of Neuroinflammation | Full Text. Accessed May 17, 2025. https://jneuroinflammation.biomedcentral.com/articles/10.1186/s12974-017-0931-5

50. Dutta K, Mishra MK, Nazmi A, Kumawat KL, Basu A. Minocycline differentially modulates macrophage mediated peripheral immune response following Japanese encephalitis virus infection. *Immunobiology*. 2010;215(11):884-893. doi:10.1016/j.imbio.2009.12.003

51. Cha GW, Cho JE, Ju YR, et al. Comparison of Four Serological Tests for Detecting Antibodies to Japanese Encephalitis Virus after Vaccination in Children. *Osong Public Health Res Perspect*. 2014;5(5):286-291. doi:10.1016/j.phrp.2014.08.003

52. Schoch CL, Ciufo S, Domrachev M, et al. NCBI Taxonomy: a comprehensive update on curation, resources and tools. *Database J Biol Databases Curation*. 2020;2020:baaa062. doi:10.1093/database/baaa062

53. Shi M, Ma G, Yang X. Artesunate: A Review of Its Potential Therapeutic Effects and Mechanisms in Digestive Diseases. *Pharmaceutics*. 2025;17(3):299. doi:10.3390/pharmaceutics17030299

54. Efferth T, Marschall M, Wang X, et al. Antiviral activity of artesunate towards wild-type, recombinant, and ganciclovir-resistant human cytomegaloviruses. *J Mol Med*. 2002;80(4):233-242. doi:10.1007/s00109-001-0300-8

55. Khanal P. Antimalarial and anticancer properties of artesunate and other artemisinins: current development. *Monatshefte Chem*. 2021;152(4):387-400. doi:10.1007/s00706-021-02759-x

56. Liu H, Li Z, Zhang Y, et al. Antiviral effects of artemisinin and its derivatives. *Chin Med J (Engl)*. 2023;136(24):2993-2995. doi:10.1097/CM9.0000000000002934

57. Ashburn TT, Thor KB. Drug repositioning: identifying and developing new uses for existing drugs. *Nat Rev Drug Discov*. 2004;3(8):673-683. doi:10.1038/nrd1468

58. Drug repurposing: progress, challenges and recommendations | Nature Reviews Drug Discovery. Accessed June 17, 2025. https://www.nature.com/articles/nrd.2018.168

59. Greenblatt W, Gupta C, Kao J. Drug Repurposing During The COVID-19 Pandemic: Lessons For Expediting Drug Development And Access. *Health Aff (Millwood)*. 2023;42(3):424-432. doi:10.1377/hlthaff.2022.01083

60. RoyMahapatra D, Singh R, Sk UH, Manna PP. Engineered Artesunate-Naphthalimide Hybrid Dual Drug for Synergistic Multimodal Therapy against Experimental Murine Lymphoma. *Mol Pharm*. 2024;21(3):1090-1107. doi:10.1021/acs.molpharmaceut.3c00632

61. da Settimo A, Primofiore G, Ferrarini PL, et al. Reinvestigation of reductive butylation of aminophthalimides: new compounds with local anesthetic activity. *Eur J Med Chem*. 1989;24(3):263-270. doi:10.1016/0223-5234(89)90008-1

62. Andricopulo AD, Müller LA, Cechinel Filho V, et al. Analgesic activity of cyclic imides: 1,8-naphthalimide and 1,4,5,8-naphthalenediimide derivatives. *Il Farm*. 2000;55(4):319-321. doi:10.1016/S0014-827X(00)00027-6

63. Muth M, Hoerr V, Glaser M, et al. Antitrypanosomal activity of quaternary naphthalimide derivatives. *Bioorg Med Chem Lett*. 2007;17(6):1590-1593. doi:10.1016/j.bmcl.2006.12.088

64. Al-Salahi R, Alswaidan I, Ghabbour HA, Ezzeldin E, Elaasser M, Marzouk M. Docking and Antiherpetic Activity of 2-Aminobenzo[de]-isoquinoline-1,3-diones. *Molecules*. 2015;20(3):5099-5111. doi:10.3390/molecules20035099

65. Perrone R, Doria F, Butovskaya E, et al. Synthesis, Binding and Antiviral Properties of Potent Core-Extended Naphthalene Diimides Targeting the HIV-1 Long Terminal Repeat Promoter G-Quadruplexes. *J Med Chem*. 2015;58(24):9639-9652. doi:10.1021/acs.jmedchem.5b01283

66. Nadai M, Doria F, Frasson I, et al. Naphthalene Diimide–Tetraazacycloalkane Conjugates Are G-Quadruplex-Based HIV-1 Inhibitors with a Dual Mode of Action. *ACS Infect Dis*. 2024;10(2):489-499. doi:10.1021/acsinfecdis.3c00453

67. Japanese Encephalitis Virus-Infected Macrophages Induce Neuronal Death | Journal of Neuroimmune Pharmacology. Accessed June 17, 2025. https://link.springer.com/article/10.1007/s11481-011-9271-x

68. Jiang W, Cen Y, Song Y, et al. Artesunate attenuated progression of atherosclerosis lesion formation alone or combined with rosuvastatin through inhibition of pro-inflammatory cytokines and pro-inflammatory chemokines. *Phytomedicine*. 2016;23(11):1259-1266. doi:10.1016/j.phymed.2016.06.004

69. Artesunate restores mitochondrial fusion-fission dynamics and alleviates neuronal injury in Alzheimer's disease models. *J Neurochem*. 2022;162(3):290-304. doi:10.1111/jnc.15620

70. Sodium Butyrate Induced Neural Stem/Progenitor Cell Death in an Experimental Model of Japanese Encephalitis | Metabolic Brain Disease. Accessed June 17, 2025. https://link.springer.com/article/10.1007/s11011-023-01279-3